Sedimentary Geology 459 (2024) 106550

Contents lists available at ScienceDirect

Sedimentary Geology

journal homepage: www.elsevier.com/locate/sedgeo

Coarse-grained submarine channels: from confined to unconfined flows in the Colombian Caribbean (late Eocene)

Sergio A. Celis [a,b,*], Fernando García-García [a], Francisco J. Rodríguez-Tovar [a,**], Carlos A. Giraldo-Villegas [a,b], Andrés Pardo-Trujillo [b,c]

[a] Departamento de Estratigrafía y Paleontología, Universidad de Granada, 18002 Granada, Spain
[b] Grupo de Investigación en Estratigrafía y Vulcanología (GIEV) Cumanday, Universidad de Caldas, Manizales, Colombia
[c] Instituto de Investigaciones en Estratigrafía-IIES, Universidad de Caldas, 170004 Manizales, Colombia

ARTICLE INFO

Article history:
Received 19 July 2023
Received in revised form 13 November 2023
Accepted 20 November 2023
Available online 25 November 2023

Editor: Dr. Catherine Chagué

Keywords:
High-density turbidites
Submarine channel-mouth bar
Supercritical flow
Cyclic steps
Antidunes
Subcritical flow

ABSTRACT

Submarine channel mouth settings are hardly preserved in the stratigraphic record. Although they are still poorly known with respect to other segments of turbidite systems, conceptual models are being refined in the light of new discoveries in modern and ancient examples. Still, some questions such as the transition between expansion zones and the traditional Channel-Lobe Transition Zone (CLTZ) remains open in ancient systems. Upper Eocene deposits of the Colombian Caribbean (San Jacinto Fold Belt) are interpreted here as a fan-delta-fed, submarine, coarse-grained channel-lobe system. It displays a well-preserved channel inception stage in the shelf break represented by sigmoidal to lens-shaped gravels, and planar cross-stratified pebbly sandstones (foreset and backset) interpreted as cyclic steps in an expansion zone. In a later stage, a classical channel-levee complex was developed, represented by channel fill elements showing sharp- and erosional-based, fining-upward sequences that are meters thick, having basal massive matrix-supported pebble conglomerates (hard—extrabasinal—clasts, rip-up clasts, coastal bioclasts), vertically evolving to liquefied massive to planar-laminated coarse-grained sandstones with phytodetrital carbonaceous laminae. They are interpreted as concentrated flow deposits (high-density turbidites) coming from continental areas or from coastal systems (i.e., delta reworking). Undifferentiated channel belt thin-bedded turbidites associated with levees and terraces deposits are related to these confined systems. The channel-lobe transition zone is characterized by debrites from cohesionless debris flow in a channel-mouth bar setting, representing bypass processes that developed distally into low-angle, planar cross- and sigmoidally-stratified (upstream antidune) pebble-size to coarse-grained sandstones that fill low-angle scours (cut-and-fill structures) in an antidune field setting with supercritical conditions. When the currents lose channel confinement, the setting is characterized by changes from Froude supercritical to subcritical flow conditions in an inner lobe to lobe off-axis environment. Large seasonal fluctuations in precipitation favor high sediment concentrations, promoting the formation of volumetrically significant fan deltas and coarse-grained submarine channels with high erosive capacity; therefore, their record helps refine interpretations of depositional processes, providing criteria for recognizing areas of the turbiditic systems that are hardly preserved. The particular aggradational conditions for the preservation and stratigraphic characterization of the rare exhumed submarine channel mouth systems make it possible to decipher sediment dispersal patterns and thus connect the models proposed here, from supercritical systems to the traditional models of turbiditic systems.
© 2023 The Author(s). Published by Elsevier B.V. This is an open access article under the CC BY license (http://creativecommons.org/licenses/by/4.0/).

1. Introduction

Submarine turbidite channel-lobe complexes have been extensively studied, revealing them to be among the most prevalent hydrocarbon reservoirs discovered in deep ocean environments (e.g., Mayall et al., 2006). Depositional elements (i.e., channel/lobe and levees) have been the main focus of many recent and ancient sedimentary systems reported in the literature, unlike the Channel-Lobe Transition Zone (CLTZ), which is still being explored (e.g., Hand, 1974; Mutti and Normark, 1987; Parker et al., 1987; Kenyon et al., 1995; Palanques et al., 1995; Wynn et al., 2002; Van der Merwe et al., 2014; Dennielou et al., 2017; Brooks et al., 2018; Maier et al., 2018). Because flows are commonly inferred to be supercritical conditions in channel to lobe

* Correspondence to: S.A. Celis, Departamento de Estratigrafía y Paleontología, Universidad de Granada, 18002 Granada, Spain.
** Corresponding author.
E-mail addresses: sergiocelis@correo.ugr.es, sergiocelis11@gmail.com (S.A. Celis), fjrtovar@ugr.es (F.J. Rodríguez-Tovar).

https://doi.org/10.1016/j.sedgeo.2023.106550
0037-0738/© 2023 The Author(s). Published by Elsevier B.V. This is an open access article under the CC BY license (http://creativecommons.org/licenses/by/4.0/).

transitional settings (Postma et al., 2021), a better knowledge of the sedimentology of supercritical flows is essential to understand the processes and their final results along the settings connecting channels and lobes. A recent revival of sedimentological studies on the supercritical flow in turbidity currents from flumes (Postma et al., 2009; Sequeiros et al., 2010; Cartigny et al., 2014; Postma and Cartigny, 2014; Lang et al., 2021; Ono et al., 2021; Wilkin et al., 2023, among others), modern systems (e.g., Fildani et al., 2006; Armitage et al., 2012; Covault et al., 2014; Hughes Clarke, 2016; Symons et al., 2016; Hage et al., 2018, among others) and outcrops (Ito et al., 2014; Postma et al., 2016, 2021; Lang et al., 2017; Ono and Plink-Björklund, 2018; Postma and Kleverlaan, 2018; West et al., 2019; Navarro and Arnott, 2020, among others) has led to a characterization of deposits from supercritical flows in terms of morphodynamics, erosional structures and bedforms (i.e., antidunes, chute-and-pools, cyclic steps).

In their wake, further studies have focused on CLTZs both in recent and ancient systems (e.g., Hofstra et al., 2015, 2018; Postma et al., 2016, 2021; Lang et al., 2017). However, the identification of channel mouth settings in the stratigraphic record is complicated by their high geomorphological dynamism and low preservation potential in modern examples (Maier et al., 2011; Hofstra et al., 2018; Hodgson et al., 2022). This has meant that facies characterization in the geologic record of these environments is still evolving (e.g., Summer et al., 2012; Postma and Cartigny, 2014; Slootman and Cartigny, 2020; Tinterri et al., 2020). A very recent classification of submarine channel mouth settings highlights the distinction between the traditional submarine CLTZ, plunge and pools, and Channel Mouth Expansion Zones (CMEZs) (Hodgson et al., 2022). CLTZs tend to be associated with abrupt breaks in slope, while CMEZs are characterized by long and broad areas of flaring of the channel and are identified where gradient changes are subtle to absent, as on a slope (Wynn et al., 2002; Navarro and Arnott, 2020; Fildani et al., 2021; Hodgson et al., 2022).

In this study, a coarse-grained unit of late Eocene age, embedded in marine muddy deposits from a forearc subduction complex (San Jacinto Formation, Colombian Caribbean; Fig. 1A-B-C) is interpreted as a channel mouth system, and proposed as an expansion zone from a confined to unconfined system, thus improving our knowledge of rare exhumed submarine channel mouth systems. The record of these deposits is therefore relevant, and together with a worldwide review of examples of various ages (China, Chile, USA, Nicaragua, Argentina, Spain), it helps to decipher depositional processes in supercritical to subcritical flows in the geological record, and moreover refines sedimentary signatures and facies, which to date have been largely based on data acquired in modern examples and tank experimentation.

2. Geological setting

The sedimentation of Colombia's Caribbean basins has been influenced by the ongoing interaction of the Caribbean Plate with the northwest margin of South America since the Cretaceous period (Pindell and Kennan, 2009; Spikings et al., 2015; Montes et al., 2019; Mora-Páez et al., 2019; Romito and Mann, 2020; Mann, 2021). Seismic data indicate that from Late Cretaceous to late Eocene times the convergence of NW South America and the Caribbean was oblique, whereas nearly orthogonal convergence has occurred from the Oligocene until the present day (Pindell et al., 2005; Villagómez et al., 2011; Bayona et al., 2012; Bernal-Olaya et al., 2015; Montes et al., 2019; Mora-Bohórquez et al., 2020). A fore-arc configuration, linked to the interaction between the Farallones and South American plates during the Late Cretaceous, is the most accepted model for the origin of this basin (Mora et al., 2017, 2018).

The San Jacinto Fold Belt (SJFB) is a SW-NE trending complex structure that forms part of the subduction complex of northwestern Colombia (Mantilla-Pimiento et al., 2009) and is located between an Oligocene to Recent fore-arc basin to the east [Lower Magdalena Valley Basin (LMVB)] and the Miocene to Recent accretionary prism to the west (Southern Caribbean Deformed Belt) (Duque-Caro, 1984; Mantilla-Pimiento et al., 2009; Bernal-Olaya et al., 2015) (Fig. 1). The SJFB represents the fossilized part of the accretionary prism of the northwest Colombia subduction complex, which today acts as dynamic backstop (Mantilla-Pimiento et al., 2009). The Romeral Fault System (RFS), which is considered to continue from the south to form the eastern boundary of the SJFB, appears to be separating the oceanic (SJFB) to transitional basement under the belt from the felsic continental basement of the South American crust, which floors the LMVB in the east (Duque-Caro, 1979, 1984; Flinch, 2003; Mora et al., 2017).

The sedimentary infill of the SJFB consists of rocks deposited from deep to shallow marine and continental settings during the Late Cretaceous to Recent, separated by regional unconformities related to tectonic events during the basin evolution (Vallejo-Hincapié et al., 2023). Deep marine environments were dominant during the accumulation of Upper Cretaceous-Paleocene rocks (Angulo-Pardo et al., 2023; Giraldo-Villegas et al., 2023; Rincón-Martínez et al., 2023). Paleocene-lower Eocene deposits have been associated with deposition from turbiditic processes, followed by a development of mixed-carbonate deposits, and finally the accumulation of coarse-grained deposits related to fan delta settings (Guzmán, 2007; Salazar-Ortiz et al., 2020b; Domínguez-Giraldo et al., 2023; Plata-Torres et al., 2023). Shelf and deltaic environments were established during the Oligocene-Early Miocene, allowing the deposition of thick muddy and sandy-carbonaceous sequences (Guzmán, 2007; Celis et al., 2021, 2023). A deepening of the basin is indicated by the regional accumulation of muddy deposits in shelf settings during the Early-Middle Miocene (Duque-Castaño et al., 2023). Shallow marine to fluvial deposits accumulated during the Late Miocene-Early Pliocene (Vargas-González et al., 2022; Ospina-Muñoz et al., 2023). Pleistocene to Recent sequences are poorly known.

2.1. San Jacinto Formation (late Eocene to early Oligocene age)

In northwestern Colombia, a regional magmatic hiatus that took place during the late Eocene-Oligocene has been associated with margin segmentation resulting from block rotation, basin opening, and deformation in other parts of the continental margin (Montes et al., 2010, 2019; Bayona et al., 2012; Cardona et al., 2012). This tectonic activity generated uplift and exhumation events of the northern regions of the Central and Western cordilleras (Restrepo-Moreno et al., 2009; Villagómez and Spikings, 2013; Cochrane et al., 2014; León et al., 2018) as well as in the basement of the adjacent basins (Mora et al., 2017; Silva et al., 2017), producing coarse-grained sedimentation in several of them and explaining the high production of detrital materials transported to the Caribbean basins by rivers at this time (Osorio-Granada et al., 2020).

Deposits prior to coarse-grained sedimentation are associated with the Chengue Formation (Fig. 1C), characterized by basinward sedimentation from the ramp, dominated by hemipelagic claystones and siltstones, and small channel-lobe systems in the outer ramp and slope (Salazar-Ortiz et al., 2020b). Later, coarse-grained siliciclastic sequence of late Eocene to early Oligocene age, deposited during the tectonic changes of the basin, is associated with the San Jacinto Formation in the SJFB (Duque-Caro et al., 1996; Clavijo and Barrera, 2001; Guzmán, 2007; Mora et al., 2017; Salazar-Ortiz et al., 2020a; Celis et al., 2023; Vallejo-Hincapié et al., 2023) (Fig. 1C). These deposits are interpreted as ancient submarine deposits in slope failures associated with fan delta environments (Duque-Caro et al., 1996; Duarte, 1997; Barrera et al., 2001). Overlying the San Jacinto Formation, El Carmen Formation (Fig. 1C) is characterized by a predominance of hemipelagic mudstones deposited in slope settings (Duque-Caro et al., 1996).

3. Methods and data set

This study is based on the sedimentological and photo-panel analysis of exposed rock formations in creeks located in the present-day onshore Colombian Caribbean region, specifically the San Jacinto

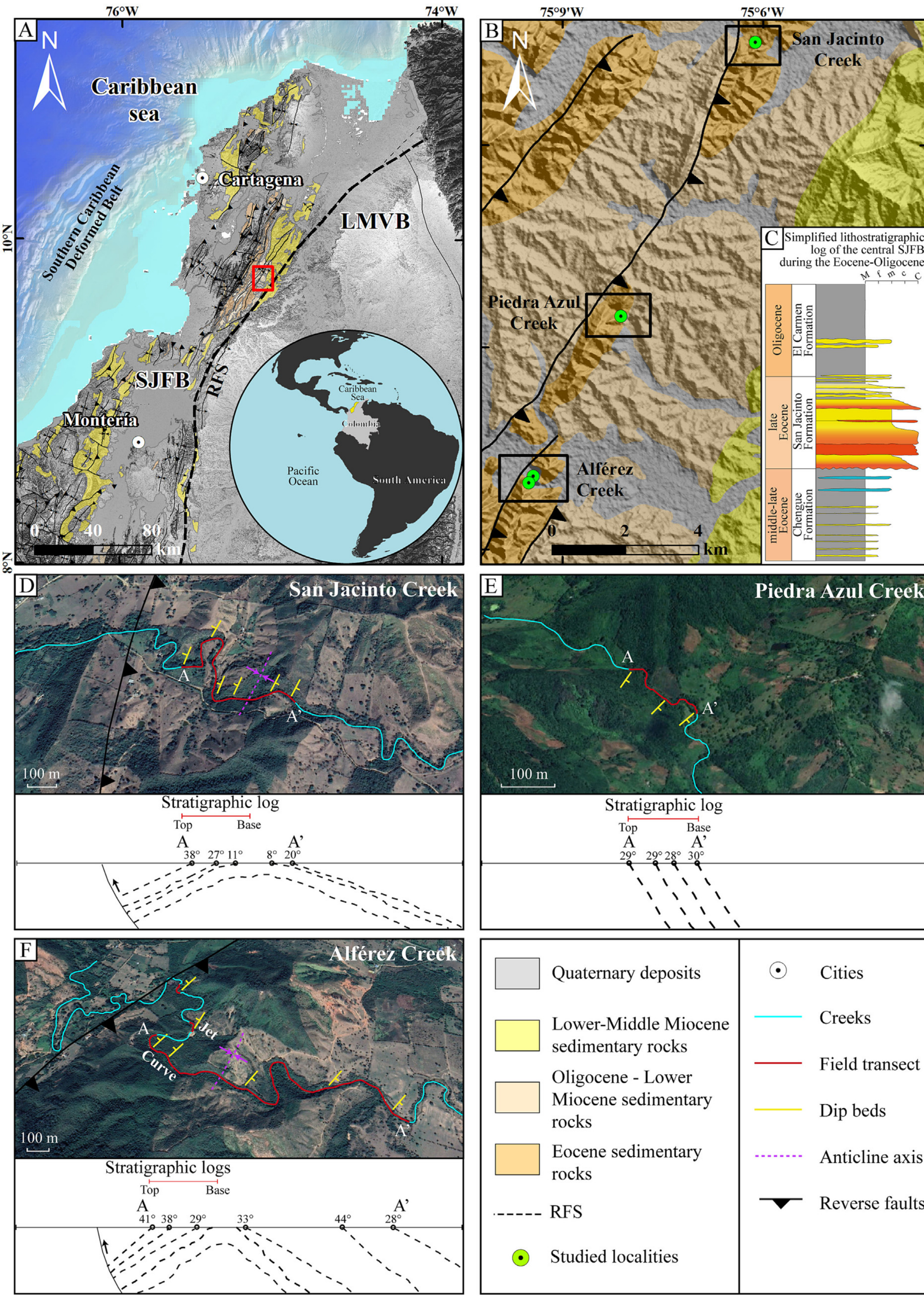

Fig. 1. A. Location map. Geological map and distribution of the Eocene to Miocene sedimentary units in Colombian Caribbean onshore basins (SJFB - San Jacinto Fold Belt; LMVB - Lower Magdalena Valley Basin; RFS - Romeral Fault System) (Source: WGS-1984 coordinate system; CIOH, SRTM, NOAA elevation, and ocean models; geology from Gómez et al., 2015). B. Location of the studied outcrops. C. Simplified lithostratigraphic log of the central SJFB with underlying (Chengue Formation) and overlying (El Carmen Formation) lithostratigraphic units. M: mudstones (gray); f: fine sandstones (yellow); m: medium sandstones (yellow); c: coarse sandstones (yellow); C: conglomerates (orange). D–F. Inset maps show details of the stratigraphic record in San Jacinto Creek, Piedra Azul Creek, and Alférez Creek (jet and curve sections).

Formation within the San Jacinto Fold Belt (SJFB) (Fig. 1D, E; Supplementary material 3). The outcrops were surveyed bed by bed using a Jacob's staff, encompassing observations of bed geometry and thickness, lithology, texture, sedimentary structures, fossils, and ichnological assemblages. Ichnological attributes such as ichnodiversity, distribution, and abundance were defined with Bioturbation Index BI sensu Taylor and Goldring (1993). Paleoflow directions were defined from planar- and trough-cross stratification, ripple-cross lamination, and clast imbrications. Bed thickness was classified as very thin (<1 cm), thin (1–10 cm), medium (11–30 cm), thick (31–100 cm), or very thick (>100 cm) according to the scheme of Nichols (2009). The gravel-clast fabric terminology used follows Walker's (1975) classification. Through the field work and photo panel analysis, the 3-dimensional arrangement of architectural elements and bounding surfaces was mapped to document the larger-scale stacking pattern of facies associations (employing the terminology of Pickering et al., 1995). Paleoflow conditions and their spatial changes and temporal evolution were taken into consideration when interpreting facies associations and stacking patterns. Biostratigraphic data were adopted from previous micropaleontological research on foraminifera and calcareous nannofossils carried out in the same stratigraphic sections in order to have an age control (e.g., Duque-Caro et al., 1996; Duarte, 1997; Guzmán, 2007; Mejía-Molina et al., 2010).

4. Results

4.1. Lithofacies and stratigraphy

Twelve lithofacies (L1 to L12) were identified and interpreted in terms of sedimentary processes in the San Jacinto Formation (Supplementary material 1). The vertical distribution of lithofacies was established through four stratigraphic logs (Fig. 2). Then, the lithofacies were grouped in seven facies associations (FA1 to FA7) and interpreted in terms of sedimentary subenvironments (Table 1).

4.1.1. San Jacinto Creek

The San Jacinto Creek section is ~84 m thick (Fig. 2). Its contacts with the underlying Chenge Formation and overlying El Carmen Formation are not recorded. The base of this section is characterized by medium to thick beds of coarse-pebble- to boulder-sized conglomerates and medium to coarse-grained sandstones. Irregular (erosive) surfaces are common, with coarse-pebble-sized conglomerates infilling scours. Additionally, thick to very thick beds having tabular and wavy geometry (boulder- to medium-pebble-sized matrix- to clast-supported conglomerates) mark irregular surfaces at the base. Embedded rip-up clasts are occasionally present. Toward the middle part of the section, flat or irregularly bounded medium to very thick beds of medium- to coarse-grained sandstones and conglomeratic sandstones are recorded, with medium- to coarse-pebble-sized clasts occurring in scour-and-fill structures. Very fine granules and coarse pebbles (up to 2 cm) are common along scour surfaces. Near the top of the section, there is a sharp contact with medium to thick beds of mudstones and fine-grained sandstones. The mean paleocurrent direction measured in planar cross-bedding sandstones and conglomerates is to the W, with some degree of variation to the W-SW and W-NW (Fig. 2).

4.1.2. Piedra Azul Creek

The Piedra Azul Creek section is ~38 m thick of exposure (Fig. 2), in which the contact with the underlying Chengue Formation is not recorded, nor that with the overlying El Carmen Formation. However, the top of San Jacinto Formation could be inferred. The San Jacinto Formation at the base of this section features a centimeter-thick intercalation of mudstones and fine- to medium-grained sandstones; a bed of cobble-sized conglomerates with normal grading to medium-grained sandstone is also observed. Above this sandstone-mudstone succession lies an irregular erosional base of medium- to coarse-grained sandstones with sigmoidal geometry. Different erosional surfaces are filled by matrix-supported cobble- and boulder-sized conglomerates (rounded to angular, poorly sorted, disorganized rip-up clasts). The matrix consists of very fine-pebble- to medium-grained sandstones. The clasts are moderately sorted, having subrounded to well-rounded cobble and coarse to very coarse pebble-sized sedimentary hard-clasts, rip-up, and bivalve gastropod fragments. Atop these successions are fine to medium sandstones, and pebble-sized conglomerates interbedding with mudstones. Rip-up clasts are imbricated to the WSW.

4.1.3. Alférez Creek

At the Alférez Creek, two sections (jet and curve) were studied (Fig. 2). The jet section is 35 m thick of exposure, in which the contact with the underlying Chengue Formation is not recorded, but the overlying El Carmen Formation is observed above a ~210 m-thick covered interval. The San Jacinto Formation at the base of this section features a decimeter-thick intercalation of bioturbated mudstones and medium- to coarse-grained sandstones having tabular geometry. The sandstones have irregular bases with load casts and asymmetric flame structures. This sandstone-mudstone succession is capped by an irregular erosional base of matrix-supported cobble- and boulder-sized conglomerates (rounded to angular, poorly sorted, disorganized rip-up clasts) commonly occurring above scour surfaces. The matrix consists of very fine-pebble- to medium-grained sandstones. Additionally, meter-scale mudstone beds are embedded within the conglomerate packages. Successive beds of conglomerates with erosive bases are recognized; they are clast-supported and moderately sorted, having subrounded to well-rounded cobble and coarse- to very coarse-pebble-sized sedimentary hard-clasts of ochre coloration. The matrix is granule to medium-grained sandstone. Atop these successions lie medium- to coarse-grained sandstones with abundant organic matter marking the laminations. Asymmetric flame structures show WSW trends; and some rip-up clasts are imbricated to the WSW.

The Alférez Creek curve section is 68 m thick of exposure and 90 m unexposed (Fig. 2). The overlying El Carmen Formation is seen above a ~90 m covered interval, but the underlying formation is not observed. This section has a base dominated by matrix-supported conglomerates, featuring coarse to very coarse to pebble-sized clasts consisting of ochre-colored sedimentary lithoclasts, and pockets of highly fragmented bivalves and gastropods. The conglomerates show fining-upward trends: from 1 to 2 m thick coarse and medium to pebble-size to very fine-pebbly sandstones and very coarse-grained sandstones, with irregular erosional bases. Toward the top, where conglomerates decrease in abundance, there are fining- and thinning-upward successions of very coarse to medium-grained sandstone with rip-up clasts, to fine-grained sandstones and mudstones with sharp and erosional bases. Bed thickness ranges from thin to thick. In some cases, thinly interbedded mudstones and very fine-grained sandstones occur at the top of the beds. Bioturbation is seen mainly at the top of the successions. The mean paleocurrent direction is to the WNW.

4.2. Facies association analysis

Seven facies associations (FA1 to FA7) were defined in the study sections (Table 1) based on the grouping of characteristic sedimentary structures, common depositional processes, stacking patterns, architectural features and temporal and spatial evolution.

4.2.1. FA1: matrix- to clast-supported, ungraded conglomerates

This facies association consists of ungraded medium to very thick sharply-based conglomerates supported by a coarse-grained sandy matrix (L1), and locally clast-supported (L2). Clasts are subrounded to subangular, granule- to pebble- and occasionally cobble-sized (Fig. 3A). Bioclasts of oysters and gastropods were recognized. Rare rip-up clasts appear with pebble-sizes (Fig. 3B). Two sub-facies associations are distinguished mainly based on the bed geometry:

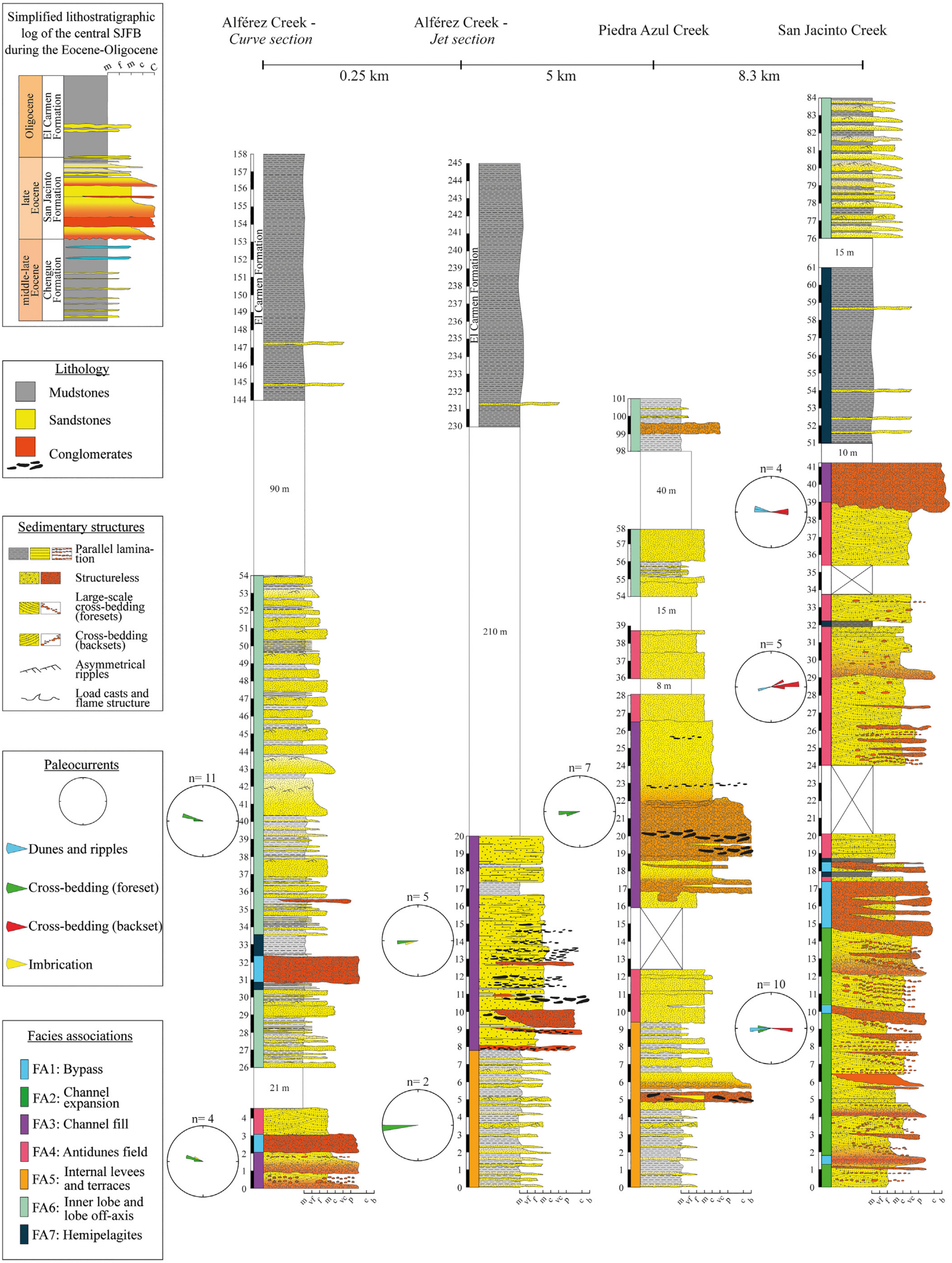

Fig. 2. Stratigraphic sections of the San Jacinto Formation.

Table 1
Facies associations and distinguishing characteristics of stratal elements.

Facies association	Order of occurrence in stratal complex	Exposed dimensions (thickness and width)	Basal surface	Sedimentary facies	Vertical and lateral trends and architectural stacking patterns	Interpretation
FA1	FA2/FA3/FA7 →FA1→ FA2/FA4/FA7	Individual: 30 cm–8 m.	Sharp and irregular.	L1, L2.	None.	Bypass.
FA2	FA1→**FA2**→FA1	Sets up to 3–8 m.	Sharp and irregular.	L1, L2, L3, L5, L6, L7, L8.	Amalgamated vertical surfaces, and grading to FA4. At the kilometer-scale, gradual lateral changes to FA3/FA5.	Channel expansion.
FA3	FA4/FA5 →FA3→ FA1	Sets up to 10 m.	Irregular.	L1, L2, L3, L4, L6, L9.	Amalgamated vertical surfaces. Upward changes in facies. Nested offset stacking. Rapid (over a few meters) lateral bed fining, and overlain to FA5.	Channel fill.
FA4	FA1/FA7 →FA4→ FA3/FA7	Sets up to 12 m.	Sharp.	L6, L7.	Vertical stacking, with subtle vertical and lateral fining and thinning.	Antidunes field.
FA5	FA5 → **FA3**	Sets up to 8 m.	Irregular.	L7, L8, L9, L10, L11, L12.	Amalgamated vertical surfaces, and erosive top to FA3. At the kilometer-scale, gradual lateral changes to FA2.	Levee/terraces.
FA6	FA7→**FA6**→FA7	Sets up to 15 m.	Irregular and sharp.	L3, L9, L10.	Vertical stacking.	Inner lobes/lobe off-axis.
FA7	FA1/FA4/FA6 →FA7→ FA1/FA4/FA6	Individual: 30 cm.	Sharp.	L12.	None.	Hemipelagites.

4.2.1.1. FA1a: sheet-like, matrix-supported conglomerate beds. This association show tabular geometry (Fig. 3C) up to 5 m thick. The basal surface is irregular (Fig. 3D), and matrix/clast ratio is low. Rare structureless rip-up clasts can be identified at the lower part (Fig. 3B), whereas the middle to upper part is well-bedded by distinct gravel and coarse- to medium-grained sandstones (Fig. 3E).

4.2.1.2. FA1b: wavy geometry, matrix-supported conglomerate beds. It shows wavy geometry (Fig. 3F, G) with thicknesses from 30 cm to 1.5 m. The basal surface is also sharply irregular. Sharp grain-size breaks occur between FA1b and the overlying FA4 (see description below) (Fig. 3F, G). It is found at the upper part of the sequences embedded into finer grain-size deposits (FA5-FA7; Fig. 3F, G). These facies show a high matrix/clast ratio.

Interpretation: Basal scour and rip-up clasts in the lower part of the beds would evidence a turbulent flow regime at the initial stage of bed deposition (Talling et al., 2012). The presence of sandstones between conglomerate beds (FA1a) in the middle to upper part of the succession marks a density-stratified flow that moved gravel as a bedload. When the traction currents declined in competence, the gravel-waves ceased to migrate, and sand that had previously been in suspension was deposited and moved as bedload while the flow was waning (Lowe, 1982; Hughes Clarke et al., 1990). FA1a and FA1b are interpreted as a debrite resulting from cohesionless debris flow, vertically evolving to surging flow (Nemec and Steel, 1984; Ge et al., 2022). The presence of sharp grain-size breaks, as seen between FA1b and FA4, allows FA1b to be interpreted as an indicator of sediment bypass (Stevenson et al., 2015; McArthur et al., 2020).

4.2.2. FA2: normally graded conglomerate lenses that transitionally evolve upward to planar cross-stratified coarse to pebbly sandstones

This facies association is represented by amalgamated thick to very thick beds of pebbly sandstones with planar cross-stratified, normal grading (L3) to fine- to medium-grained sandstones, convex-up low-angle surfaces (L5, L7), and mound-shaped geometries. The arrangement can be divided into three parts according to textural variations (Fig. 4 general view and sketch general view). The lower (1–2 m thick) consists of lens-shaped conglomerates with extra-pebble clasts (rip-up clasts are absent), having massive structure (L1), diffuse low-angle and planar cross-stratified, and sigmoidal geometry infilling convex-up erosional surfaces where rare load casts are present (Fig. 4A, B, and sketch B). Typically, clast- or matrix-supported conglomerates (L1, L2) with subrounded to well-rounded pebbles to cobbles —mostly derived from sedimentary rocks— make up the basal scour infills. Upward, the middle part contains thicker beds (2–4 m thick) of sigmoidal cross-stratified pebbly sandstone deposits (L7; Fig. 4D) that laterally may pass into lens- and mound-shaped beds of pebbly sandstones with low-angle, trough and planar cross-bedding (L6, L7; backsets- and foresets; Fig. 4C–E, and sketch C). Just upstream, lens-shaped, massive to crudely planar cross-stratified pebbly sandstone occurs (Fig. 4D). The enclosing facies of the mound-shaped beds consist of coarse- to medium-grained sandstones and pebbly sandstones that appear trough cross-stratified (asymptotic downstream) (Fig. 4E). Structureless and weakly-bedded sandstone (L8) deposits occur in the upper bed (top), up to 1 m thick (Fig. 4C and sketch C).

Interpretation: Altogether, the prevalence of convex-up surfaces, scour-and-fill structures, planar cross-stratified pebbly sandstone, lens-shaped geometry with backsets and foresets, and subsequent draping of these surfaces by onlapping of asymptotic downstream cross-bedding pebbly sandstones (Fig. 4F) would be associated with a supercritical high-density turbidity current that generated small cyclic steps (Cartigny et al., 2014; Hage et al., 2018; Slootman and Cartigny, 2020). Massive or crudely laminated zones just upstream of the lens-shaped beds could be associated with the hydraulic jump (Postma and Kleverlaan, 2018). Scour fills display crude and widely spaced low-angle stratification, indicating a decrease in sediment concentration and an increase in bedload transport and bed shear stress; it could occur rapidly downflow of the hydraulic jump, where a velocity maximum causes higher boundary shear stress and thus more erosive power (Sequeiros, 2012; Postma and Cartigny, 2014). This transition may take place swiftly downstream of the hydraulic jump (Postma and Cartigny, 2014; Postma et al., 2014; Lang et al., 2017). In the mound-shaped beds, the migration of the crest occurs at an angle of climb that exceeds the dip of the lee side (Fig. 4D, and sketch D), resulting in an overall aggradational state on both sides of the step. This allows the preservation of continuous beds across cyclic steps, appearing as wave trains in the depositional record (Vellinga et al., 2018; Slootman and Cartigny, 2020). They are classified as 'fully depositional cyclic steps' following Slootman and Cartigny (2020), in this case formed under high values of sediment concentration, where amalgamation shows that fine sediment deposition is prevented in the upper part of the bed. Deposition in fully depositional cyclic steps occurs from the leeward side in foreset-bedding and aft side in backset-bedding (Slootman and Cartigny, 2020). However, the angle of

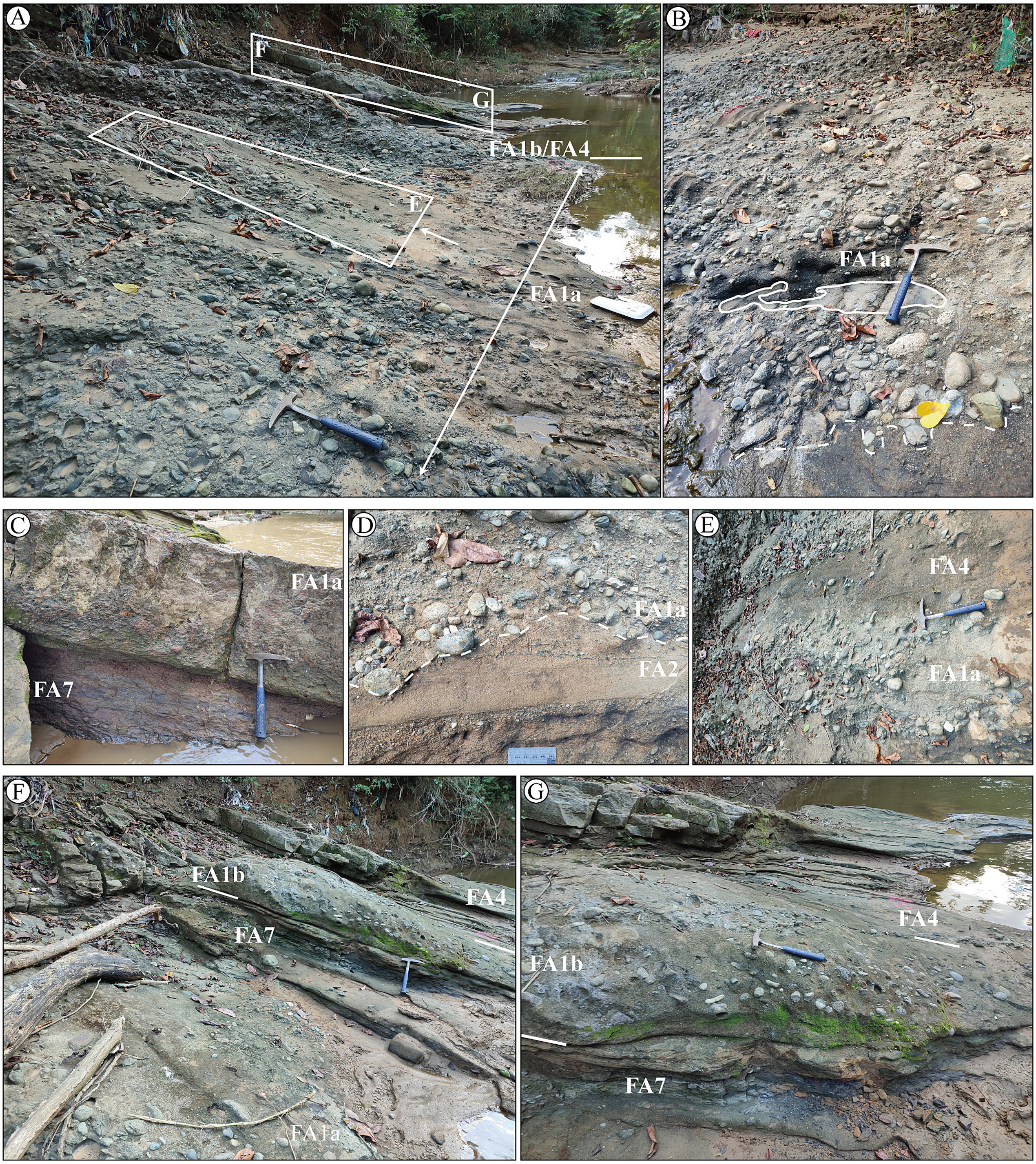

Fig. 3. Facies association 1 (FA1). A. Section showing the vertical transition from matrix-supported rounded pebble clasts (FA1a) to sigmoidally cross-stratified coarse-grained sandstones (FA4) capped by sigmoidal-shaped, matrix-supported conglomerate beds (FA1b) (at the top of the picture) (hammer is 32 cm long). B. Large rip-up clasts in the lower part of the matrix-supported rounded pebble clasts (FA1a) overlying FA2 through irregular contact. C. Mudstones (FA7) in sharp irregular contact with tabular bed of matrix-supported conglomerate (FA1a). D. Detail of the irregular base (dashed line) of the matrix-supported rounded pebble clasts (FA1a) (chart to scale: 10 cm). E. Sandstone-dominated layers in the middle-upper part of the matrix-supported rounded pebble clast beds (FA1) (see location in panel A). F–G. Sigmoid-shaped, matrix-supported conglomeratic beds (FA1b) interbedded with sigmoidally cross-stratified granule to coarse-grained sandstones (FA4) and horizontally laminated dark mudstones (FA7) (see location in panel A).

migration of the climb that exceeds the dip on the lee side is not perfectly preserved; therefore, the lee side could have been eroded —the rate of sediment removal being less than the rate of deposition on the stoss side— and the cyclic steps could have been partially depositional (Slootman and Cartigny, 2020).

The bases of slope breaks, when there are gradient changes at the basin bottom (continental slopes and related canyons), appear to favor either already subcritical flows or swift transitions from supercritical to subcritical flow conditions (e.g., Fildani et al., 2021; Hodgson et al., 2022). Although the bedforms developed in the expansion zones are generated by turbidity currents in upper flow regimes, the aggradational and preservation tendencies must occur beneath supercritical to subcritical flows (*Fr* close to 1) to prevent erosion (Postma et al., 2016; Hodgson et al., 2022).

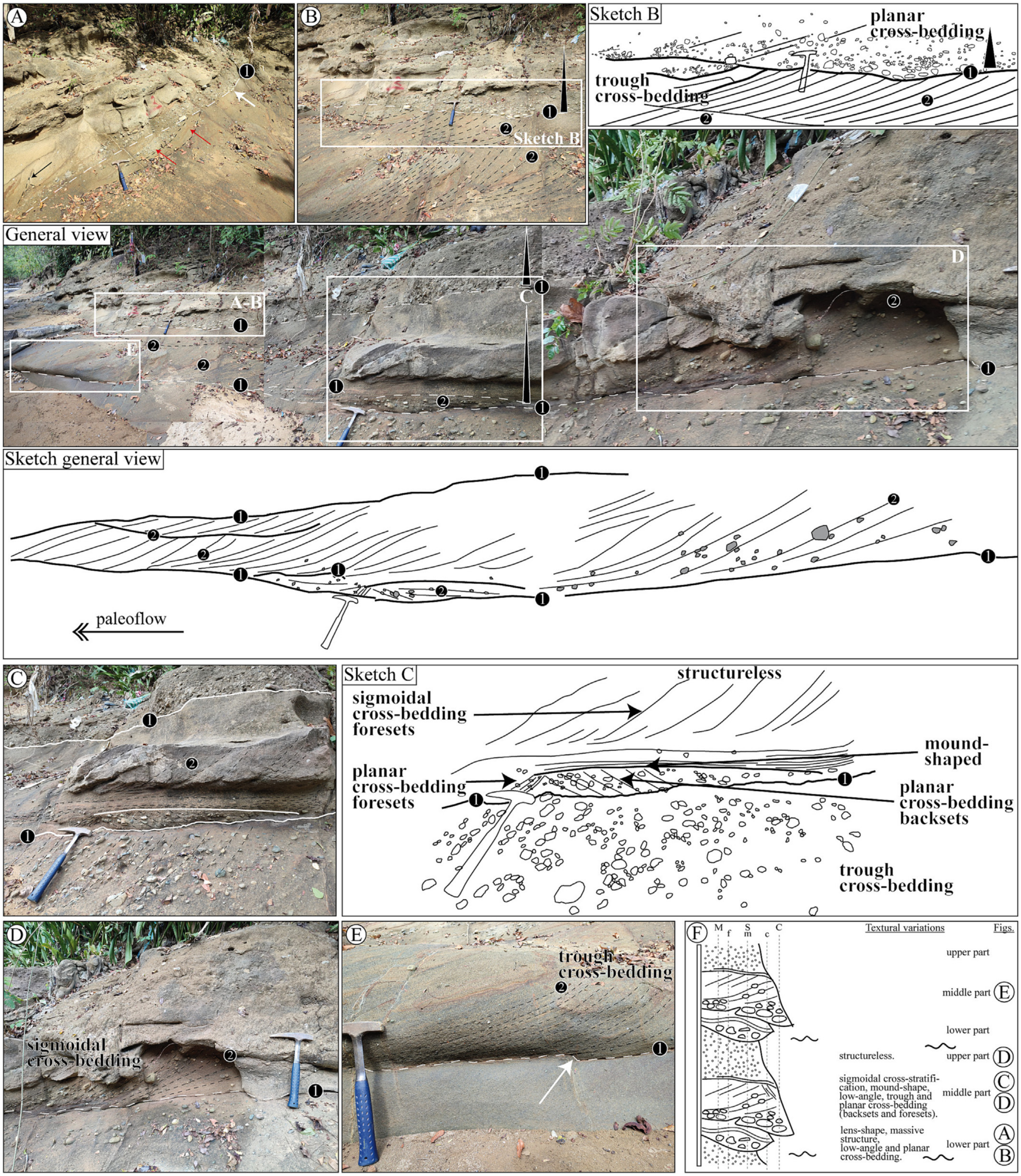

Fig. 4. Facies association 2 (FA2). General view and sketched general view of the lower part of the San Jacinto Creek section. Two-meter-thick pebbly sandstone beds appear amalgamated. The amalgamation surface stratigraphy hierarchy is marked by numbers: 1. Cross-bedding coset stratigraphic surfaces, 2. cross-bedding set stratigraphic surfaces (hammer is 32 cm long); (see figure locations in General view). A. Lens-shaped and mound-shaped structures of normal-graded gravels and sandstone deposits (red arrows), flame structure (black arrow) intruding into structureless sandy upper interval, and sigmoidal gravel deposits infilling a shallower and longer scour (white arrow). B and sketch B. Detail and line drawing of the lower part deposits. Note the erosional, scoured basal surface truncating underlying planar cross-bedded sandstones. Gravels show diffuse planar cross-bedding (dipping toward the left) with scattered pebbles dispersed in sand-dominated laminae. C and sketch C. Detail and line drawing of the middle part deposits. Mound-shaped with backset-bedded pebbly sandstone deposits cap the amalgamation surface, and a sigmoidal cross-bedded sandstone unit encloses the mound-shaped ones. D. Lens of pebbly sandstone deposits at the lower part of the sigmoidal cross-bedded unit. It appears overlying the amalgamation surface (dashed line). E. Trough cross-bedded sandstones with scattered very fine and coarse pebbles. F. Schematic textural variations for FA2.

4.2.3. FA3: graded and amalgamated matrix-supported conglomerates to sandstones

This association is represented by vertical and nested offset stacking, irregular and sharply-based conglomerates supported by a medium- and coarse-grained sandy matrix, massive and occasionally graded (L3) to sandstone deposits. Two sub-facies associations are distinguished in view of the stacking pattern and sedimentary structure:

4.2.3.1. FA3a: vertical stacking, normally-graded, rip-up- and/or hard-clast conglomerates to sandstones. This is represented by lenticular-shaped geometry and medium to thick beds, normally graded, consisting of three intervals (Fig. 5): i) A lower interval exhibiting hard-clast- and matrix-supported conglomerates with some angular rip-up clasts (L1, L2, L3; Fig. 5A, B), ii) a sharp-based, planar-bedded granule- to very-coarse-grained sandstone (L9) interval in the middle part (Fig. 5A, B), and iii) an upper interval characterized by planar cross-bedded upstream (backsets) very fine-pebble-size to sandstone deposits (L6; Fig. 5C, D).

Interpretation: These deposits forming upward-fining sequences represent the channel fill at the channel axis (Kane et al., 2009). Angular rip-up clasts indicate that these deposits are relatively immature, and they could evolve downslope into fully turbulent flow where sediment would break up (e.g., Mulder and Alexander, 2001; Kane et al., 2009).

4.2.3.2. FA3b: nested offset stacking, amalgamated scour-and-fill, rip-up- and/or hard-clast conglomerates to sandstones. Coarse-grained lags that include mudstone breccia with frequent deformed shale clasts are overlain by amalgamated thick-bedded conglomerates and sandstones (L1, L2, L4, nested offset stacking; Fig. 6). Scours are 0.5 m deep and 2–15 m long (Fig. 6A, and sketch A), and are mostly irregular and asymmetrical. Scour fills consist of matrix-supported conglomerates (L1) with pebbly sandstone or coarse- to medium-grained sandstone as matrix, as well as bivalve and gastropod fragments (Fig. 6). In some cases, the bases of the larger scours are characterized by deposits associated with FA5, having scoop-shaped and smaller-scale scours (see below in FA5). The composition of the clasts filling the scours can be divided into rip-up (Fig. 6B) and hard (Fig. 6C), while in rare cases rip-up and hard clasts are mixed. Rip-up clasts consist of mudstone and siltstone ranging from coarse-pebbles to cobbles and rare boulder size (up to 0.40 m in diameter; Fig. 6D), subangular to subrounded. The hard clasts range from very fine pebbles to coarse pebbles, subangular to angular, ochre-colored, derived sedimentary rocks. The clast fabric is commonly random. In general, the coarsest grain sizes occur within the largest scours with rip-up clasts, and even partially complete layers can be part of the backfill (Fig. 6D, E). Internally, the rip-up and hard-clast scour fills are massive; rip-up clast scours fills are amalgamated. Yet appearing upward in the succession are normally-graded rip-up clasts that are pebble- to cobble-size with imbrication to the SW (L3; Fig. 6F), along with horizontally laminated coarse- to medium-grained sandstones with plant debris (L9; Fig. 6G).

Fig. 5. Facies association 3a (FA3a). A. Sharp-based, normally-graded conglomerate to sandstone deposits (FA3a) (hammer is 32 cm long). B. Detail of the lower conglomeratic interval in panel A exhibiting clast-supported fabric and normal grading with scattered large clasts at the top (arrow). Note the sharp transition between conglomeratic and overlying granule and sandstone intervals (lines) (scale = 10 cm). C–D. Vertical transition from planar-bedded to backset planar cross-bedded (dashed lines) fine-pebble size conglomerates to sandstone intervals (see location in panel A). Sharp transition (lines separating a lower brown interval from an upper gray one) between intervals could indicate an amalgamation surface between two different depositional events or surges of an unstable flow. Lasting would support the vertical decrease in grain size (hammer is 32 cm long in both pictures).

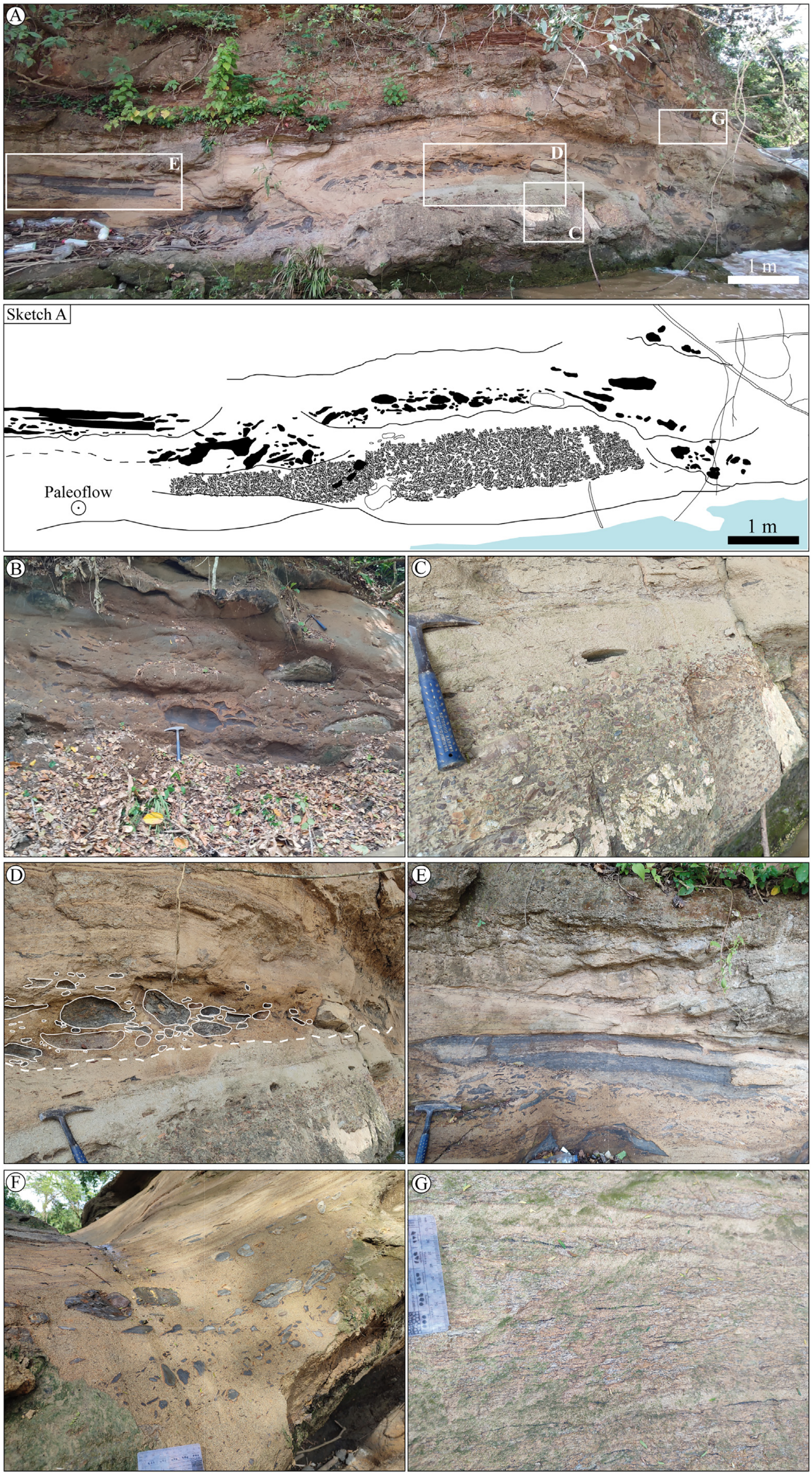
A
E
D
C
G
1 m
Sketch A
Paleoflow
1 m
B
C
D
E
F
G

Interpretation: Amalgamated coarse-grained scour fills indicate erosion by a high-velocity water flow, and subsequent filling by subangular to subrounded intraclasts from highly concentrated flows that represent significant sediment bypass or a waning phase of the flow that cuts the scour (Postma et al., 1988, 2014; Peakall et al., 2020). In submarine channels, the occurrence of vigorous substrate scouring and ripping-up of partially complete beds, coupled with the subsequent deposition of unstructured beds, suggests an explosive hydraulic jump phenomenon (Postma et al., 2009). The occurrence toward the top of normal grading beds rich in laminated plant debris may be associated with hyperpycnal flows delivered directly from subaerial settings (Lowe, 1976; Zavala and Pan, 2018; Zavala, 2020; Grundvåg et al., 2023).

4.2.4. FA4: sigmoidally stratified pebbly sandstones

This facies association is represented by 15–30 cm thick, coarse-tail, normally-graded to low-angle, sigmoidal cross-stratified pebbly to granule sandstone beds (Fig. 7A, B). Scours are filled by asymmetrical lenticular beds of foresets and concave-up, low-angle backset planar cross-stratified pebbly to granule sandstones (Fig. 7C, D). The dimensions of the lenticular to sigmoidal elements are characterized of low amplitude (5 cm) and relatively long wavelength (30–50 cm) (Fig. 7E, F). Laterally the thickness pinches and swells slightly due to converging-diverging stratification (Fig. 7E, F). Asymmetrical sigmoidal stratified sandstones (e.g., humpback cross-bedding-type) also appear (Figs. 7E, F).

Interpretation: Low-angle backsets and foresets in gravel sandstones are interpreted as representing deposits of low relief antidunes and chutes or pools due to internal waves, surges or unstable hydraulic jumps (Lang and Winsemann, 2013; Ono and Plink-Björklund, 2018). Humpback dunes are interpreted as dune to upper plane bed transitions in open channel flows (i.e., river channels, Fielding, 2006). However, supercritical flow experiments in density flow showed that humpback dunes may also represent downslope migrating antidunes with high rates of deposition (Lowe, 1982; Fielding, 2006; Lang and Winsemann, 2013; Fedele et al., 2016; Winsemann et al., 2021). The lack of upper plane beds in these deposits (which would be common in supercritical flows occurring in open channel flows; Fielding, 2006) could signal that the density flow did not reach the high Froude numbers required for upper plane beds (higher than the open channel flow analogs, as reported by Fedele et al., 2016 experiments). Thus, this facies association is interpreted as the result of an aggrading antidune-type bedform in granule to coarse-grained sand beds. It would have formed under supercritical flows, as observed in laboratory flumes (e.g., Alexander et al., 2001; Fedele et al., 2016; Ono and Plink-Bjorklund, 2018; Winsemann et al., 2021). Steep scours filled by foreset and backset planar cross-bedding are interpreted as the result of breaking waves (Ono and Plink-Bjorklund, 2018). The absence of plane bed zones laterally separating antidunes discounts their stability where flow becomes transcritical (from supercritical flow at relatively low Froude numbers; Cartigny et al., 2014). Here they are capped by cut-and-fill (antidune) structures, thus implying rising flow power conditions during supercritical flow, or deposition by waxing flows that attain supercritical flow conditions (Lowe, 1982; Saunderson and Lockett, 1983; Chakraborty and Bose, 1992; Fielding, 2006).

4.2.5. FA5: burrowed (Ta-e) sandstone and mudstone layers

This facies association comprises interbedded thick to very thick sheet-like beds of massive mudstone, and fine- to medium-grained sandstone beds (L10, L11, L12; Fig. 8A, B, C) with massive (L8), horizontally laminated (L9), planar cross-bedding (L7), and ripple lamination structures, as well as normal grading (L10), having erosional bases that often contain load casts and flame structures (Fig. 8C, D, E). Sandstones present moderate ichnodiversity, low to moderate abundance (BI = 1–3), and show *Ophiomorpha* and *Thalassinoides* (Fig. 8E), while the mudstones show patches of *Nereites* and *Phycosiphon* and locally *Taenidium* (Figs. 8F, G), with moderate ichnodiversity and a moderate to high intensity of bioturbation (BI = 3–4). The top of these successions is overlain by erosional surfaces associated with FA3, which contains abundant rip-up clasts (Fig. 8D).

Interpretation: Thick to very thick beds of fine-grained sandstones are attributed to sediment deposition along the channel margin areas (such as internal levees and terraces) where the low-concentrated turbidity flows slow, or because the flow thickness is greater than the channel depth, or because of inertia at channel bends or in encounters with irregularities, leading to escape from the main channel, and sometimes even the formation of minor channels (Kane and Hodgson, 2011; Pickering and Hiscott, 2015; Bayet-Goll et al., 2023). The distinction between inner levees and terraces requires a well-defined channel belt architecture; so, in our study we consider these systems as undifferentiated channel belt thin-bedded turbidites (according to Hansen et al., 2015).

The presence of trace fossils such as *Ophiomorpha* and *Thalassinoides* could be related to the *Ophiomorpha rudis* ichnosubfacies within the *Nereites* ichnofacies, associated with deposition from turbidity currents by the channel (Uchman, 2009; Uchman and Wetzel, 2012). In an internal levee and terrace setting, interbedded bioturbated mudstones tend to settle out of suspension under lower-energy conditions from clouds of overflowing turbidity currents, or due to hemipelagic processes when the system shutdown (Heard and Pickering, 2008; Kane and Hodgson, 2011; Hansen et al., 2015). *Nereites* and *Phycosiphon* must be related to *Nereites* ichnosubfacies in the *Nereites* ichnofacies, common in lower energy environments or associated with muddy flysch sediments (Uchman and Wetzel, 2012; Callow et al., 2014; Rodríguez-Tovar, 2022). It should be noted that the distribution and abundance of these ichnological associations vary in the presence of cohesive debris flow, which forces organisms to migrate from areas of higher energy to areas where low-density turbidites predominate (Hubbard et al., 2008, 2012; Callow et al., 2014; Bayet-Goll et al., 2023).

The observed sedimentary pattern could be the first stage of an abandonment drape, caused by a number of factors, such as upstream channel avulsion, relative sea-level rise, or changes in the sediment supply brought on by tectonic activity or climate shift in the source area (Clark and Pickering, 1996; Richards et al., 1998).

4.2.6. FA6: prograding successions decreasing from coarse, conglomeratic sandstones to bioturbated mudstones

This facies association is characterized by tabular fining- and thinning-upward successions from conglomeratic sandstones to mudstones that are up to 2 m thick and show sharp and irregular erosional bases (L3, L10; Fig. 9A, B, C, and sketch B). Occasionally, scours are infilled by gravel and coarse sandstone, or the basal beds are granule- to pebble-sized matrix-supported conglomerates, with primarily lithic sedimentary angular clasts and a medium-grained sandy matrix. Rare grooves and flute marks are observed. Metric packages of poorly sorted medium-grained sandstones with pebble-sized rip-up clasts also occur, predominantly distributed at the bases of the successions. In some cases, this succession is repeated, showing erosive bases. In other layers, however, normal grading (L10) to medium to fine-grained sandstones with horizontally lamination (L9) are observed, followed by sandstones with ripple lamination and planar cross-lamination toward the top (Fig. 9D, and sketch D). Synsedimentary deformation structures are sometimes found (Fig. 9D). The

Fig. 6. Facies association 3b (FA3b). A and sketch A. Cross-section of the top of the Alférez Creek (jet section) showing amalgamation of rip-up- and hard-clast channels with high organic content. B. Abundant concentration of rip-up clasts with boulder-sized particles. C. Coarse-grained turbidite channel composed of hard sedimentary lithics, with massive structure and normal grading at the top. D. Abundant concentration of rip-up clasts at the base of the channel, with boulder-sized particles overlying another channel consisting of hard clasts. E. Concentration of rip-up clasts and whole bed fragments ripped off the previous basin floor, forming a basal lag deposit. F. Rip-up clasts ranging in size from pebbles to cobbles floating in a medium-grained sandy matrix. Some clasts show SW imbrication. Chart to scale: 10 cm. G. Abundant layers of organic matter highlighting parallel lamination toward the top of the accumulation of rip-up clasts, emphasizing normal grading in the succession. Chart to scale: 10 cm.

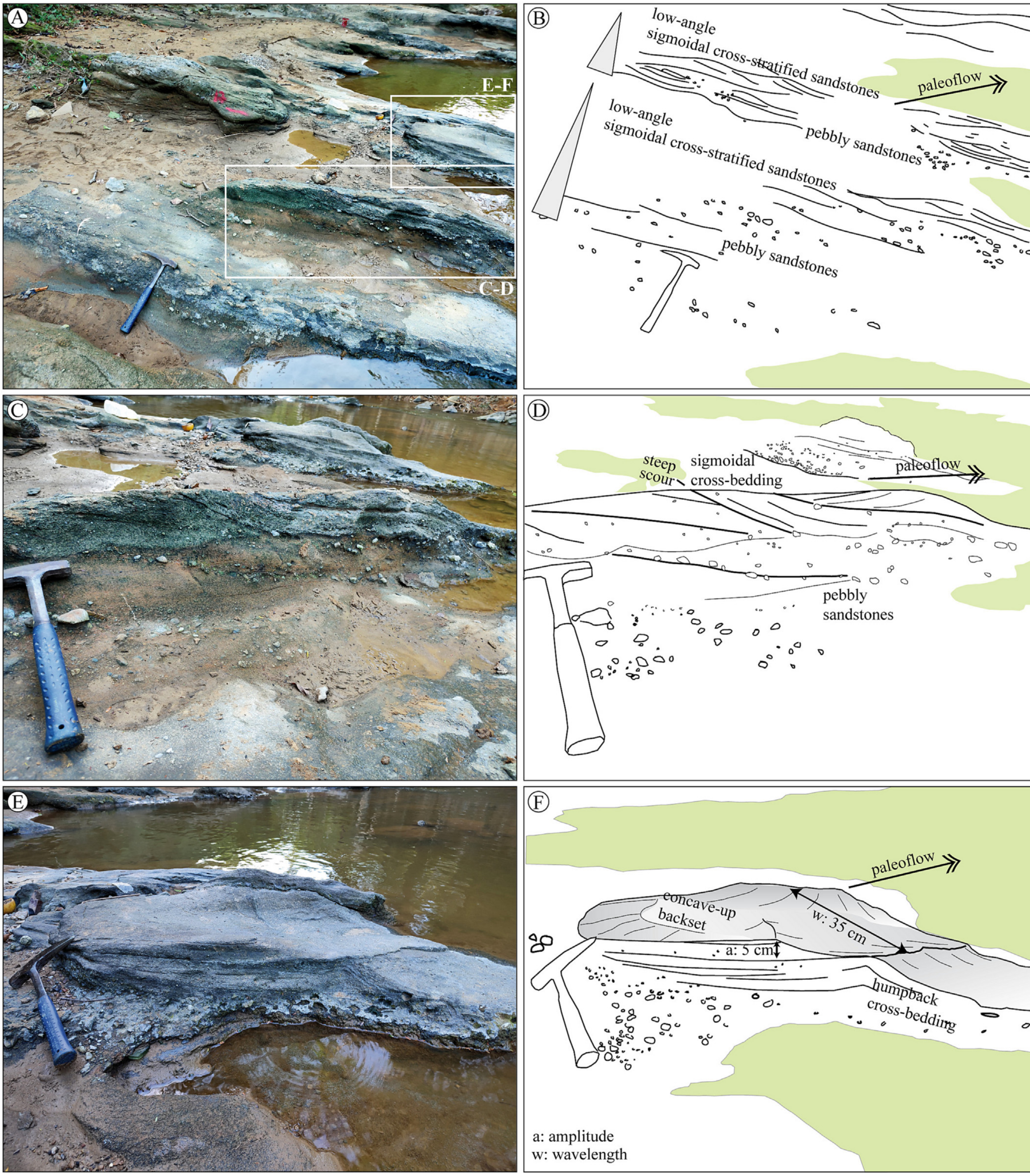

Fig. 7. Facies association 4 (FA4). A–B. Field picture and line drawing showing normally graded, vertical stacking of centimetric-thick, low-angle cross-laminated pebbly sandstone to sandstone beds. See panel A for location of detailed photos C and E. C–D. Field photo and line drawing showing a lens of gently sigmoidal cross-bedded pebbly sandstone and asymmetrical cross-laminated granule to sandstone bed with scouring and filling structure interpreted as unstable antidune (see text for details), E–F. Field picture and line drawing showing gently backflow cross-bedded and humpback cross-bedding sandstone at the top of a pebbly sandstone bed interpreted as antidunes (see text for details) (32-cm long hammer to scale in all the pictures).

tops of the successions are bioturbated mudstones with *Ophiomorpha*, *Scolicia*, *Taenidium*, and *Thalassinoides* (Fig. 9E).

Interpretation: The repetition of tabular bedding, erosional basal bed surfaces, and rip-up clasts suggest the presence of high-energy turbiditic currents generating scours prior to deposition, where angular sedimentary clasts indicate a nearby source (Brooks et al., 2022). Normal grading is often associated with the waning stage of turbidity currents — the decrease in flow velocity would allow sediment particles to settle out of suspension, transitioning from depositional to bypass conditions (Komar, 1985; Kneller and Branney, 1995; Kneller and Buckee, 2000;

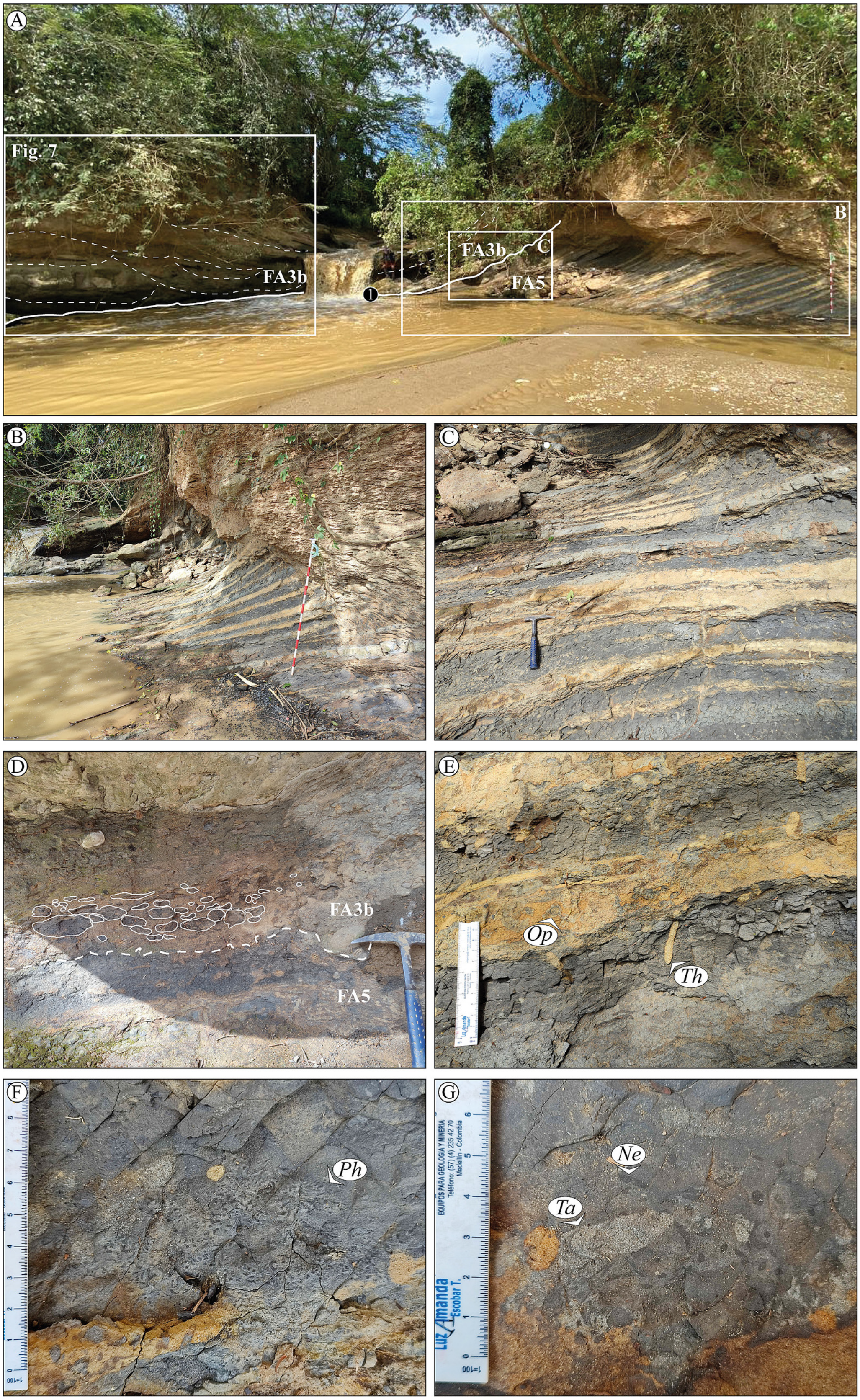

Fig. 8. Facies association 5 (FA5). A. General view of the internal levee/terrace succession (FA5), overlain at the top by an erosive surface associated with the turbiditic channel (FA3b). B–C. Interbedding between massive bioturbated mudstones and fine- to medium-grained sandstones with ripple lamination, parallel lamination, and erosive basal surfaces highlighting load-cast structures. Jacob's Staff for scale: 1.5 m. D. Irregular (erosive) surface of a submarine channel overlying internal levee/terrace deposits (FA5), with reworking of rip-up clasts. E. Irregular erosional basal surface of fine-grained sandstone with abundant ripple lamination and intense bioturbation by *Ophiomorpha* (*Op*), *Thalassinoides* (*Th*) toward the top. The contact with massive bioturbated mudstones displays a gradational transition. F-G. Massive bioturbated mudstones with patches of abundant *Phycosiphon* (*Ph*) and *Nereites* (*Ne*), showing cross-cutting relationships with *Taenidium* (*Ta*).

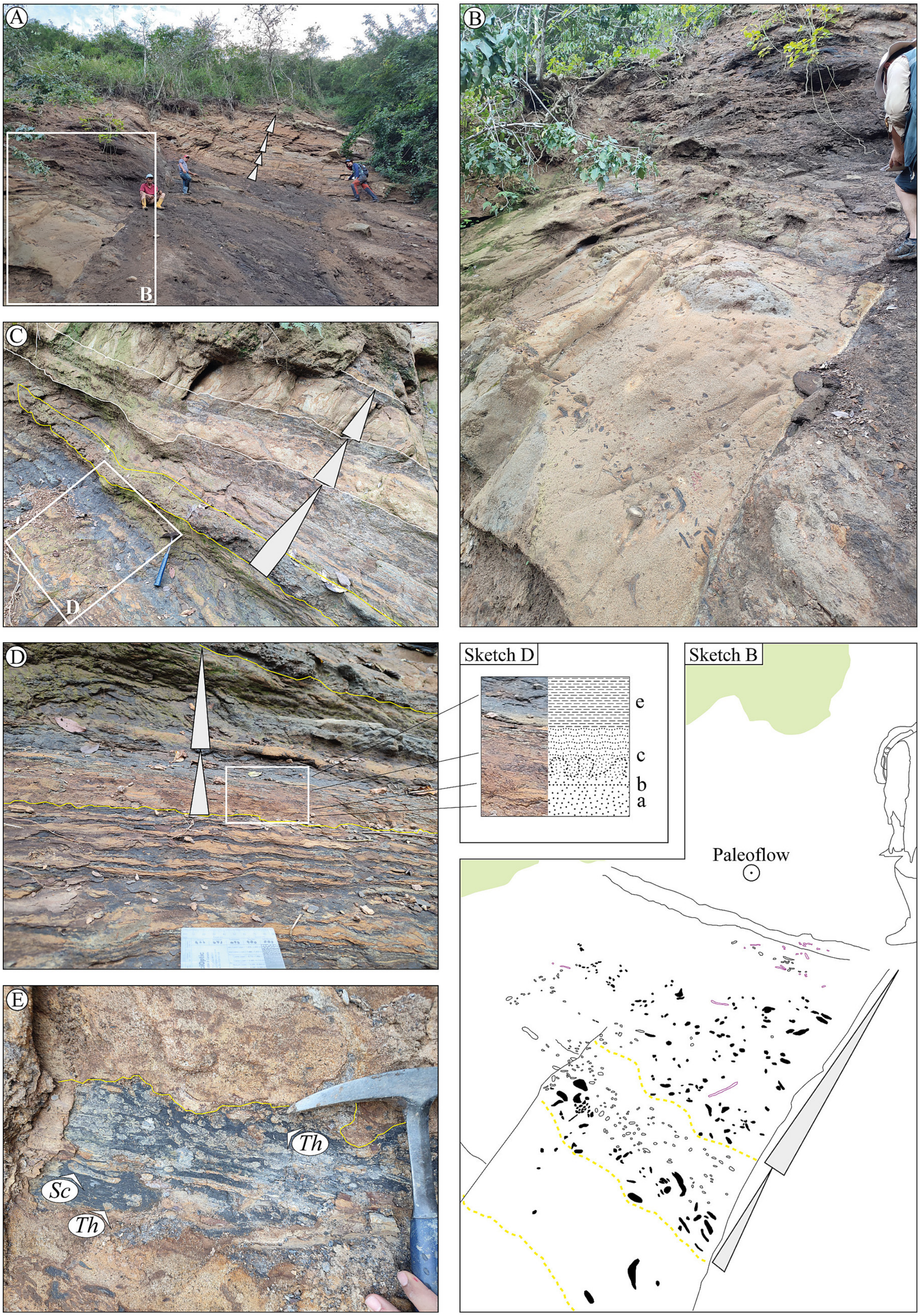

Fig. 9. Facies association 6 (FA6). A. Overview of the outcrop. B. Erosional surface and deposit of medium- to coarse-grained structureless sandstone with accumulations of rip-up clasts and subsequent fining-upward successions (see sketch B). C. Fining- and thinning-upward successions ranging from poorly sorted granule-sized conglomerates that are matrix- to clast-supported, passing transitionally to medium- to coarse-grained sandstone and upward fine-grained sandstone and mudstone. Topping beds are generally bioturbated. D. Ripple lamination is detailed at the base. Irregular surface and detail of the fining-upward succession from massive medium-grained sandstone (a), transition to a zone of *syn*-sedimentary deformation (b), upward ripple lamination (c), and bioturbated mudstones (e) (see sketch D). Chart to scale: 10 cm. Detail of the top of the fining-upward succession consisting of bioturbated mudstone with *Scolicia* (*Sc*) and *Thalassinoides* (*Th*), in addition to unidentified trace fossils.

Kneller and McCaffrey, 2003; Stevenson et al., 2014). Fine-grained sandstones with parallel lamination toward the base, followed by a development of planar cross-stratification, could indicate transport by a not very strong current of traction. Convolute laminations may be produced by shear, buoyancy instabilities, and/or water escape (e.g., Allen, 1977, 1985; Gladstone et al., 2018), indicating high suspension fall-out rates. Laminated fine-grained silt and mud accumulate toward the top when the flow is very slow and close to stopping. *Ophiomorpha*, *Scolicia*, *Taenidium* and *Thalassinoides* at the top indicate a post-depositional trace fossil assemblage assigned to the *Ophiomorpha rudis* ichnosubfacies, commonly found in channels and/or proximal lobes of turbidite systems (Uchman, 2009; Uchman and Wetzel, 2012; Callow et al., 2014; Rodríguez-Tovar, 2022). Therefore, beds with gradations to finer sediments, as well as the presence of Bouma divisions, amalgamated sandstones, bioturbation to the top, laterally adjacent channel fills, and fining- and thinning-upward sequences would be indicative of the waning phase of low-density turbidity currents, suggesting deposition between an inner lobe and lobe off-axis context (Hubbard et al., 2009). The amalgamated massive sandstones and conglomeratic sandstones suggest rapid sediment deposition in marginal sheets of channels by turbidity currents of lower density in internal levees; when there is insufficient space in the channel for the flow to decelerate and deposit most of its sediment before reaching the channel boundary topography, confined sheet deposits or terraces are created (e.g., Babonneau et al., 2004; Kane and Hodgson, 2011; Paull et al., 2013; Hansen et al., 2015).

4.2.7. FA7: dark-gray mudstones

This facies consists of sheet-like beds of massive to horizontally laminated gray mudstones and siltstones (L12), 20–30 cm thick, with a few thinner interbedded horizontally-laminated siltstones, 3–5 cm (Fig. 3C–F, G). They contain mainly agglutinated benthic foraminifera.

Interpretation: Massive mudstone was deposited by suspension, settling in a low-energy environment attributed to hemipelagic sedimentation on the basin floor, where parallel-stratified mudstone beds are associated with low-energy traction-plus-fallout processes of low-concentration turbidity currents (Stow and Piper, 1984; Stow, 1985; Stow and Tabrez, 1998; Potter et al., 2005; Navarro and Arnott, 2020; Stow and Smillie, 2020).

5. Depositional model

The studied sections of the San Jacinto Formation in Caribbean Colombia consist of predominantly coarse-grained deposits interpreted as the result of highly concentrated flows that occurred during the late Eocene. They would range from cohesionless debris flows to high-density turbiditic currents that persist in both supercritical to subcritical conditions (and transitions in between). The cyclic steps (FA2), antidune field (FA4), fining-upward successions (FA5 and FA6), reworking of fossil fragments from coastal systems (FA3b), benthic foraminiferal assemblages (FA7) associated with outer shelf to upper bathyal environments (Duque-Caro et al., 1996; Guzmán, 2007; Garzón Oyola, 2023), and the high content of organic matter (FA3b) all lead us to interpret that the flows with supercritical conditions were confined in submarine slope channel complexes that evolved into less confined areas along well-preserved channel mouth depositional settings, with a final transformation to subcritical flows in an inner lobe to lobe off-axis context (Figs. 10, 11).

5.1. Stage 1

The lower section in San Jacinto Creek is dominated by deposits of high-density currents in supercritical conditions represented by cyclic steps (FA2). The initiation is marked by depositional cyclic steps in an expansion zone along a shelf break to continental slope from confined flows (CMEZ using the classification of Hodgson et al., 2022) (Figs. 10, 11).

Sedimentary features of the deposits (amalgamation, lack of fine deposits, poorly sorted deposits, and subangular rip-up and extra clast-dominated deposits; FA1 and FA2) indicate that highly concentrated flows were confined within this submarine transfer routing system; therefore, it recorded the inception of a submarine channel (i.e., slope channel) fed directly from continental settings (i.e., alluvial fans or steep rivers) (Fig. 11).

They are preserved as bypass deposits at the channel thalwegs, representing amalgamated infill units at the axis of these channels (Fig. 11). The presence of gravel lenses and planar cross-stratified coarse-grained sandstone and conglomerate lag facies—as described here— are interpreted to represent bypass in slope channel fills (Mutti, 1992; Stevenson et al., 2015). Confined high-energy flows over a steep slope would impede the deposition of muds draping amalgamation surfaces, as reported in gentler base-of-slope settings (e.g., Mutti and Normark, 1987).

Cyclic steps (lower section in San Jacinto Creek) below and adjacent to stacking channel elements (Piedra Azul Creek, and upper part of Alférez Creek – jet section) would record the overall progradation of a lower slope succession, as interpreted in other ancient records (e.g., Pemberton et al., 2016) (Figs. 10, 11). Channel fill elements are interpreted as cohesionless debris flows (bypass) and concentrated flow deposits (high density turbidites), likewise derived directly from continental areas or from a reworking of coastal systems (i.e., delta). The fine-grained sediment fraction of the flows was deposited outside of the channel belt as undifferentiated thin-bedded turbidites associated with levees or terraces (FA5) (Figs. 10, 11).

5.2. Stage 2

Confined deposits in expansion zones (supercritical flows) vertically evolve to sigmoidal lens-shaped gravels, foreset and backset planar cross-stratified pebbly sandstones, and low-angle upstream, undulated-stratified (antidunes) granule to coarse-grained sandstones filling gentle scours (cut-and-fill structures) (FA4), which would represent the transition from CMEZ to CLTZ (San Jacinto Creek) (Figs. 11, 10). Coarse-grained mouth-bar migration and antidunes (FA4) linked to supercritical flows characterize the CLTZ, where the currents lose channel (or canyon) confinement in the mouth to antidune field setting. However, the occurrence of sporadic debrites and channel fill toward the middle part of the San Jacinto Creek section (FA1), as well as interbedding with hemipelagites in a mixed-foraminiferal assemblage (FA7) with species typical of the outer shelf to upper and middle bathyal zones (Duque-Caro et al., 1996; Guzmán, 2007) would indicate other periods of slope instability (Fig. 10).

The increased tabular bedding and fining-upwards successions, from coarse conglomeratic sandstones to bioturbated mudstones (FA6; Piedra Azul Creek and Alférez Creek – curve section) probably overlapping or adjacent to an antidune field (San Jacinto Creek) may support a progressive decrease in depositional energy, which is associated with waning phase of low-density turbidity currents, suggesting deposition between an inner lobe and lobe off-axis context (Figs. 10, 11).

Thus, the complete stratigraphic succession of San Jacinto Formation exposes the initiation, progradation and then retrogradation of a coarse-grained turbidite channel-lobe system (Figs. 10, 11).

The studied sections of this lithostratigraphic unit are interpreted as the expression of decreasing confinement along a coarse-grained, submarine sediment routing system (Fig. 11). It transferred highly concentrated flows from coarse-grained coastal systems (i.e., fan delta) to deep-water settings. Similar and scarce slope evolution has been documented in view of recent and ancient examples (e.g., Pemberton et al., 2016; Brandes and Winsemann, 2018).

6. Discussion - from confined to unconfined flows in coarse-grained channels: assessing integrative sedimentary facies

The CLTZ is perhaps the geomorphic subregion having the least available data among modern and ancient turbidite systems given its

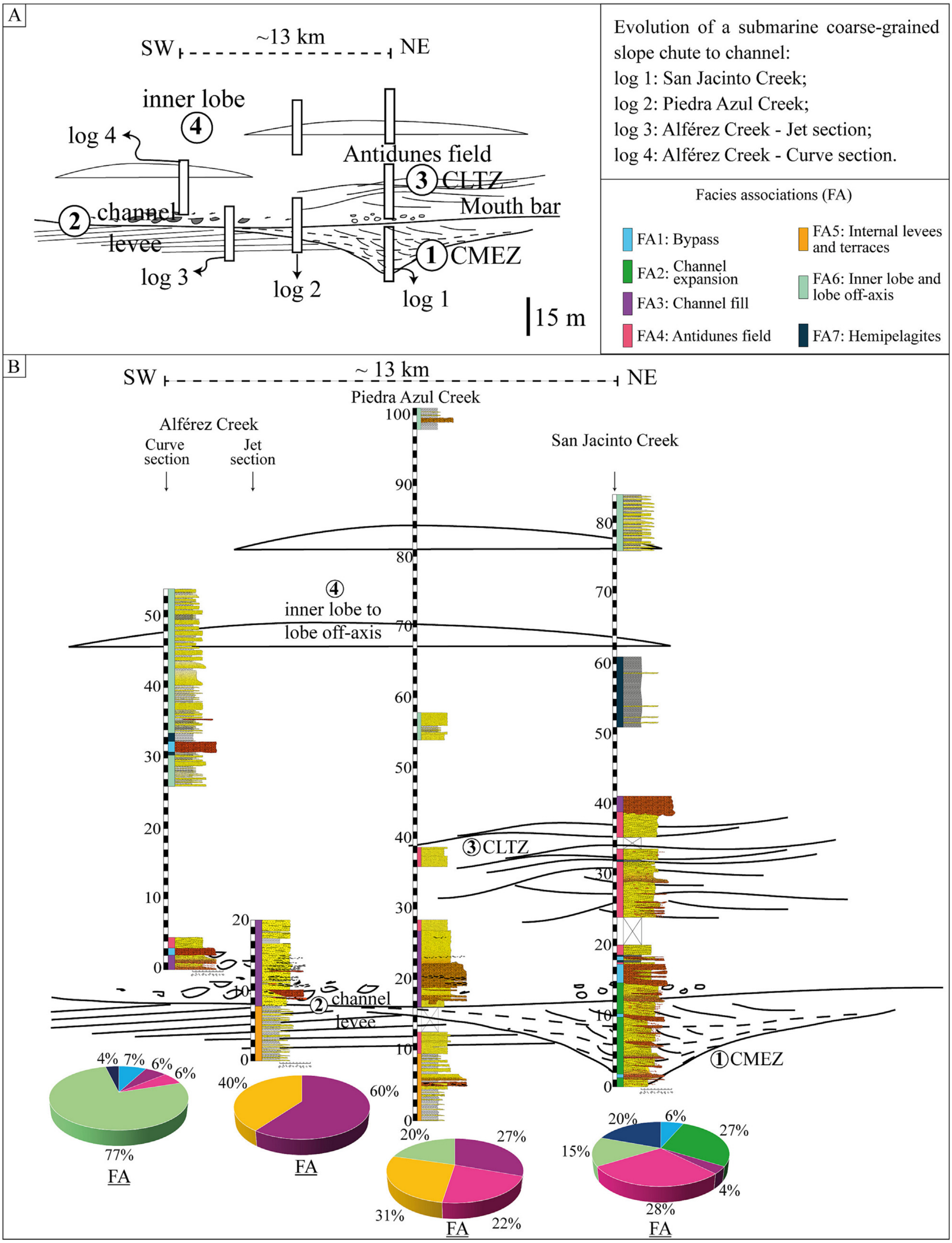

Fig. 10. A–B. Sketch cross-section showing dominant facies associations and bedforms of the stage of expansion zone (CMEZ according to Hodgson et al., 2022) from proximal to distal settings, marking a stratigraphic correlation between San Jacinto Creek (to the north), Piedra Azul Creek, and Alférez Creek (the curve section and the jet section, to the south) based on sedimentary features recognized in outcrops. Note that the lower part of the sequence (1. CMEZ) is reported only in the San Jacinto Creek; 2. representative channel-levee elements in Piedra Azul Creek and Alférez Creek (the jet section); 3. antidune field and debrite bypass associated with CLTZ as reported in San Jacinto Creek and Piedra Azul Creek; and toward the top, 4. Inner lobes to lobe off-axis recognized in San Jacinto Creek, Piedra Azul Creek and Alférez Creek (curve section).

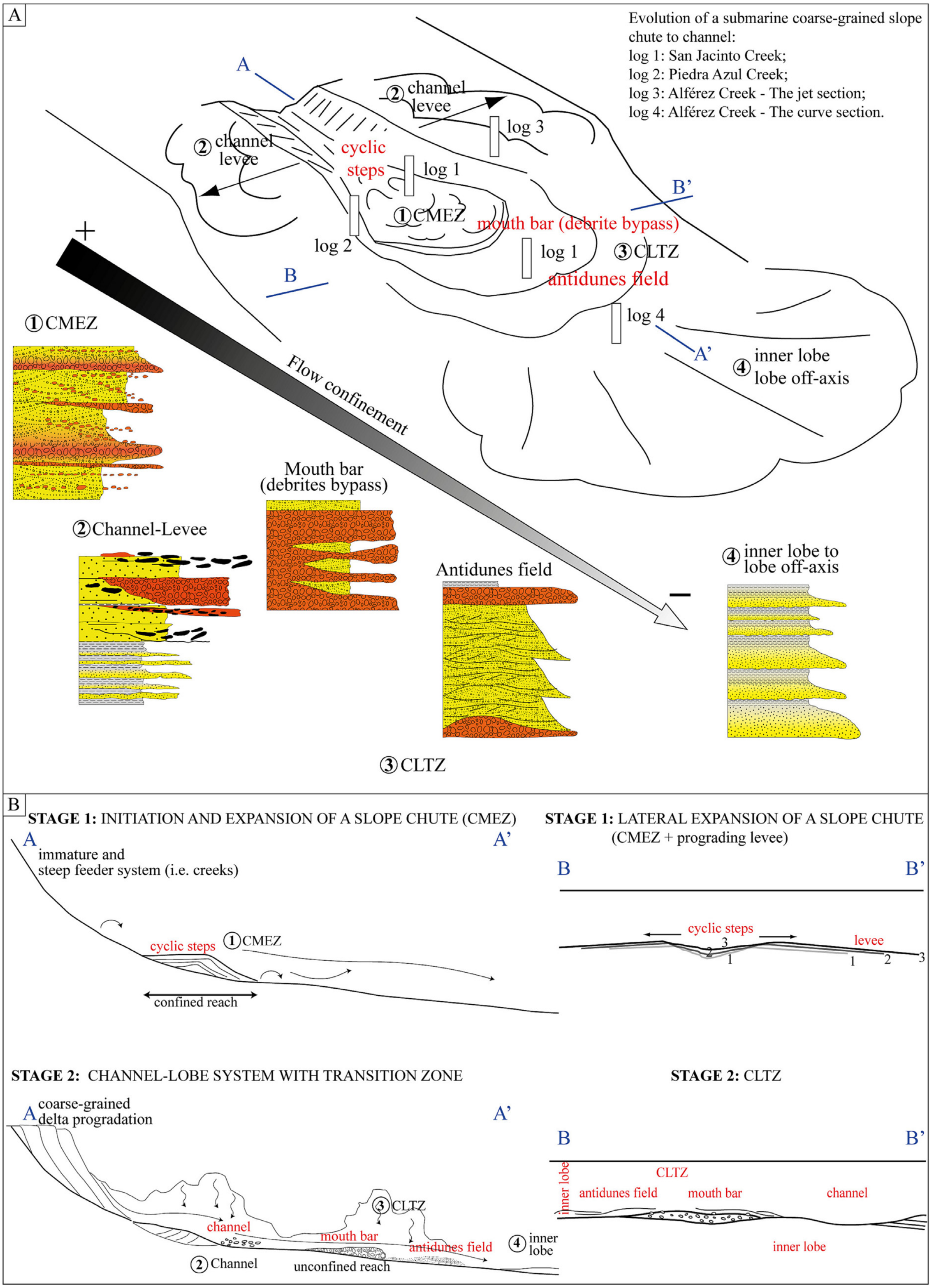

Fig. 11. A. Supercritical to subcritical flows from CMEZ to classical CLTZ. Sedimentary facies. B. Cross-sections (A-A′ and B-B′) along and perpendicular to the channel axis showing different dominant sedimentary structures from channel-confined proximal settings (cyclic-step-dominated) to unconfined distal settings (inner lobes to lobe off-axis).

high erosive capacity, resulting in poor preservation (Hand, 1974; Mutti and Normark, 1987; Parker et al., 1987; Kenyon et al., 1995; Palanques et al., 1995; Wynn et al., 2002; Van der Merwe et al., 2014; Dennielou et al., 2017; Brooks et al., 2018; Maier et al., 2018; Maestrelli et al., 2020). As a result, knowledge of these zones is still developing worldwide, and their identification in outcrops is challenging. Studies of both modern examples and outcrops have led to new classifications (e.g., Hodgson et al., 2022). While descriptions to date of CLTZs include plunge pools, and distinctive long and flared tracts between channels and lobes, the novel term Channel Mouth Expansion Zone (CMEZ) has been proposed by Hodgson et al. (2022). Fitting these deposits into facies models is nonetheless complex, due to the multiple scenarios that can be generated (e.g., Postma et al., 2014). Multiple allogeneic and autogenic factors modify the CLTZs: basin architecture (in active or passive margins); tectonic activity such as subsidence and uplift; sediment supply; weathering processes; amount of rainfall and runoff; temperature and sea-level changes; or sediment transport pathways from the source area. Therefore, the morphology and architecture of CLTZs depend on internal and external factors of the basin and the function of the Froude (*Fr*) number, with supercritical CLTZs differing from subcritical examples (Postma et al., 2016; McArthur et al., 2020).

Considering the sections visited and previous reports, we consider that this expansion zone would have a width of about 10 km (from San Jacinto Creek and transition to Piedra Azul Creek), with a channel lobe transition area of about 5 km (from Piedra Azul Creek to Alférez Creek); channel fills related to the backfilling phase have lenticular geometries with widths of <100 m (Piedra Azul Creek and Alférez Creek). However, we lack sufficient outcrops to establish the full continuity of the transition zones or interactions with other systems. Although this expansion system seems small in comparison with other examples (see Navarro and Arnott, 2020), it must be taken into account that it corresponds to a single system and that other systems probably developed along the margin. This study is one of the few that reflects the expansion and then decrease of confinement along a coarse-grained sediment routing system. The compilation of different facies associations and other outcrop examples from deep-sea environments elsewhere (Supplementary material 2; China, Chile, USA, Nicaragua, Argentina, Spain) allows us to characterize at the facies level certain expansion zones and transitions to CLTZ under the domain of high-density turbidity currents fed by supercritical flows that transition to subcritical flows at active margins (Supplementary material 2).

6.1. Mouth expansion zone

By studying the evolution of the San Jacinto Formation, several arguments can be derived about sedimentary systems and factors increasing the likelihood of preservation of ancient expansion zones [CMEZs according to Hodgson et al., 2022] in the sedimentary record. It is recorded at the base (stage 1 of the channel evolution) of a submarine channel-lobe system dominated by highly-concentrated flows (cohesionless debris flows and high-density turbidity currents) coming directly from the continent with coastal reworking (fossil fragments, abundant sheets of organic matter). Thus, low-angle, upstream and downstream planar cross-bedding pebbly sandstones (back- and foresets) as well as lens- and mound-shaped beds characterized supercritical flows; but near the boundary subcritical flows occurred at the beginning of the slope chute to channel dynamics (Fig. 11). Coarse grained submarine slope systems (from submarine canyons to slope channel and fan complexes) composed of deposits of high-density turbidity currents are commonly related to short and steep margins with abrupt relief close to the shoreline, or high-gradient alluvial-fluvial systems (i.e., fan deltas, Gilbert-type delta, shelf-edge deltas) attached to them. In this case, they may have been fed by products from the erosion of mountain range systems that show contemporaneous faster cooling rates along the entire paleomargin, related to exhumation and/or uplift during the final magmatic shutdown in the late Eocene (e.g., Restrepo-Moreno et al., 2009; Villagómez and Spikings, 2013). This would constitute one of the first evidences of coarse-grained deposits associated with the western margin of the orogen, and could become further evidence that the cooling of the margin is indeed related to exhumation-erosion.

Coarse-grained submarine slopes derive from tectonically-active settings such as forearc basins (e.g., La Jolla Group; Maier et al., 2020, or Otadai Formation; Brooks et al., 2022) and from passive-margin contexts (e.g., Azpiroz-Zavala et al., 2017; see review in Navarro and Arnott, 2020). Tectonically active margins, generally with steep gradients and high sediment supply, provide a landscape where strong Froude supercritical flow turbidity currents can occur (e.g., Supplementary material 2; Ono and Plink-Bjorklund, 2018). This study strongly supports that tectonically active basin fills—such as the Colombian Caribbean forearc basin—represent a favorable host of expansion zones given their steeper slopes than those of relatively tectonically-quiescent ones. In addition, aggradational cyclic steps resulting in bed amalgamation in expansion zones (see FA2) require variability in river discharge, favored by the tropical humid conditions that involved large seasonal fluctuations in rainfall during which the deposits were formed (e.g., Martínez et al., 2021).

Hence, early-stage successions having a high proportion of supercritical bedforms and erosion surfaces could be candidates for sedimentary facies of expansion zones (Supplementary material 2; Postma et al., 2014; Gong et al., 2017; Lang et al., 2017; Cornard and Pickering, 2019; Postma et al., 2021). Notwithstanding, some examples of early expansion zone stage candidates could be from aggradational systems, where the onset of flow at lobe initiation stages may entail antidune facies associations and subsequently initiate a prograding cycle associated with cyclic steps (e.g., Supplementary material 2; Postma and Kleverlaan, 2018; Postma et al., 2021).

6.2. Channel-levee complex

Amalgamated scour-and-fill, rip-up- and/or hard-clast conglomerates to sandstones with nested offset stacking, and burrowed (Ta-e) sandstone and mudstone layers below and adjacent to the expansion zone represent channeled high-density turbidites, as well as its levees and terraces, marking the onset of gravity flow deconfinement/transit.

Other examples of high gradient slopes and confined settings are known to form the feeder systems that subsequently generate large- and small-scale cyclic steps (e.g., Supplementary material 2; Ponce and Carmona, 2011; Postma et al., 2014, 2021; Cornard and Pickering, 2019). Apart from tectonics, climate is an important factor contributing to the development of the channel-levee complex and expansion zones, as highly concentrated flows coming directly from the continent are generated by river floods (e.g., Gábris and Nagy, 2005; Vellinga et al., 2018). Variable discharge rivers have been shown to support high sediment concentrations, promoting the formation of volumetrically significant fan deltas and coarse-grained submarine channels (Gábris and Nagy, 2005; Wagreich and Strauss, 2005; Lang et al., 2017; Yang et al., 2017; Brandes and Winsemann, 2018; Grundvåg et al., 2023). On many occasions, this variability generates re-accelerated flow in the first stages of amalgamation of cyclic steps, hence a repetition of hydraulic jumps from supercritical to subcritical, and back to supercritical flows (e.g., Supplementary material 2; Lang et al., 2017). Although no repetitions or variations in the cyclic steps could be identified here, the tropical context would favor such scenarios of systems fed by hyperpycnal flows (Supplementary material 2; Yang et al., 2017; Martínez et al., 2021). Coarse- to medium-grained sandstones with inverse and then normal grading, horizontally laminated with plant debris (FA3b), are considered diagnostic facies of hyperpycnal flow origin (Mulder et al., 2003; Zavala et al., 2011, 2012; Yang et al., 2017; Grundvåg et al., 2023).

6.3. CLTZ: mouth bar (debrite bypass and antidune field)

CLTZs are the passage zones between channel-levee systems and well-defined lobes (Hansen et al., 2021; Hodgson et al., 2022). Therefore, they encompass facies associations with depositional and erosional bedforms ranging from cyclic steps to antidunes. Yet using the new classification by Hodgson et al. (2022) and based on the literature review, our study proposes integrative sedimentary facies from confined to unconfined systems. Accordingly, CLTZ would be linked to the second stages of supercritical bedforms, and characterized by sigmoid-shaped centimeter-thick, normally-graded pebbly sandstone to medium-grained sandstone deposits having sigmoidal symmetrical or asymmetrical cross-bedding; low-angle bedding at the top with humpback cross-bedding capped by sheet-like and lenticular-like matrix-supported conglomerate beds represent the progressive deconfinement of the flow in a transition zone between supercritical to subcritical flows ($Fr \sim 1$). The vertical stratal stacking pattern of the succession is another key to explain the low preservation of the expansion zones (CMEZ, according to Hodgson et al., 2022) in the ancient record. Candidate San Jacinto expansion zone and other outcrops (i.e., Supplementary material 2; Ponce and Carmona, 2011; Postma et al., 2014; Gong et al., 2017; Lang et al., 2017; Yang et al., 2017; Ono and Plink-Bjorklund, 2018; Postma and Kleverlaan, 2018; Cornard and Pickering, 2019) are preserved at the base of a succession exhibiting a retrogradational pattern represented from bottom to top by a candidate expansion zone-channel/levee, and initial stages of unconfinement in CLTZ (Fig. 11; Supplementary material 2; Postma et al., 2014; Pemberton et al., 2016; Lang et al., 2017; Cornard and Pickering, 2019). Perhaps the most documented prograding slope settings are not very favorable for expansion zone preservation because of a highly erosional depositional history, meaning the transit of flow decelerations to the antidune field is often not well preserved (Supplementary material 2; Ponce and Carmona, 2011; Pemberton et al., 2016; Postma et al., 2016; Gong et al., 2017). Furthermore, in some zones the first stages of the flow may be completely aggradational (antidune), but progradation begins later (e.g., Postma and Kleverlaan, 2018; Postma et al., 2021).

6.4. Overbank to inner lobes

A prograding stacking pattern of successions—decreasing from coarse, conglomeratic sandstones to bioturbated mudstones— is associated with the zones best preserved in the stratigraphic record, and on this basis the facies models of channel-lobe transition zones in deep marine environments are put forth (Postma et al., 2014; Brooks et al., 2022). Typical successions with gradual energy decay —often bioturbated at the top under subcritical conditions in a deconfined state— have allowed us to observe numerous study sequences (e.g., Summer et al., 2012; Postma and Cartigny, 2014; Tinterri et al., 2022). Even facies models and stacking patterns of fine-grain sizes under supercritical conditions have been proposed (Normark et al., 2009; Mukti and Ito, 2010; Postma and Cartigny, 2014; Postma et al., 2014). In this case, however, such successions represent the end of the retrograding pattern, and link the previous facies with models established outside the confined channel suggesting deposition between an inner lobe and lobe off-axis.

7. Conclusions

Coarse-grained deposits of the San Jacinto Formation (late Eocene, Colombian Caribbean forearc subduction complex) are interpreted to record an exceptionally complete history of inception and evolution of a submarine channel system dominated by cohesionless debris flow to high-density turbidity currents with highly variable (Froude number) flow conditions. Gravelly amalgamated depositional cyclic step sets developed by highly concentrated flows in supercritical conditions are related to the onset of the confined segment becoming a submarine channel. Laterally, beyond the expansion zone (CMEZ), an aggrading undifferentiated channel belt thin-bedded turbidites associated with levees and terraces complex is built. Distally evolving to the expansion zone, bypass debrite capped by antidunes alternating with mudstone layers can be interpreted as the slope channel-mouth bar and the antidune field of a Channel-Lobe Transition Zone (CLTZ) dominated by cohesionless debris flows to high-density turbidites under supercritical conditions. Finally, the transition to the subcritical domain is determined by the record of bioturbated inner lobe to lobe off-axis deposits. The stratigraphy of the San Jacinto Formation in this area reflects an expanding and then decreasing confinement along a coarse-grained sediment routing system, from the channel mouth expansion zone to channel-lobe transition zone in the shelf-break context. Clast textural features, abundant organic matter, and reworked coastal bioclasts found within the coarse-grained deposits reveal that the head of the slope channel/canyon cuts across a shallow marine system fed by a fairly high-gradient fluvial system and immature source. This occurred along a tectonically-active, short and abrupt basin margin, with seasonal rainfall variations during the Eocene-Oligocene transition in the forearc subduction complex. The development of expansion zone deposits in the form of cyclic steps takes place in the framework of concurrent active sediment transport, bypass, and deposition of coarse-grained material from a channel-levee system; the antidune field (transition from expansion zones) and loss of confinement in inner lobes to lobe off-axis context are compared with further examples of deep marine environments having expansion zones. Thus, the facies evolution proposed here can be linked with traditional facies models in turbiditic systems, to propose advances in our knowledge of the transition from supercritical to subcritical flows.

Supplementary data to this article can be found online at https://doi.org/10.1016/j.sedgeo.2023.106550.

Data availability

Data will be made available on request.

Declaration of competing interest

The authors declare that they have no known competing financial interests or personal relationships that could have appeared to influence the work reported in this paper.

Acknowledgments

Financial support of Celis and Giraldo-Villegas was provided by the National Program for Doctoral Formation (Minciencias Colombia grants 885-2020, 906-2021 respectively). Financial support for Rodríguez-Tovar was provided by scientific Projects PID2019-104625RB-100 (funded by MCIN/AEI/10.13039/501100011033), P18-RT-4074 (funded by FEDER/Junta de Andalucía-Consejería de Economía y Conocimiento), B-RNM-072-UGR18 and A-RNM-368-UGR20 (funded by FEDER Andalucía). We would like to express our gratitude to Catherine Chagué (Editor-in-Chief) and two anonymous reviewers for their constructive comments and suggestions. Funding for open access charge: Universidad de Granada / CBUA.

References

Alexander, J., Bridge, J.S., Cheel, R.J., Leclair, S.F., 2001. Bedforms and associated sedimentary structures formed under supercritical water flows over aggrading sand beds. Sedimentology 48, 133–152.
Allen, J.R.L., 1977. The possible mechanics of convolute lamination in graded sand beds. Journal of the Geological Society 134, 19–31.
Allen, J.R.L., 1985. Principles of Physical Sedimentology. George Allen and Unwin, London (272 pp.).
Angulo-Pardo, E., Vallejo-Hincapié, F., Do Monte Guerra, R., Pardo-Trujillo, A., Giraldo-Villegas, C.A., García Gonzáles, J., Hernández Duran, S., Herrera Quijano, S., Plata Torres, A., Trejos-Tamayo, R., 2023. Late cretaceous calcareous nannofossil assemblages from Colombia: biostratigraphic contributions to northwestern South American Basins. Journal of South American Earth Sciences 127, 104315. https://doi.org/10.1016/j.jsames.2023.104315.
Armitage, D.A., McHargue, T., Fildani, A., Graham, S.A., 2012. Postavulsion channel evolution: Niger Delta continental slope. AAPG Bulletin 96, 823–843.
Azpiroz-Zavala, M., Cartigny, M.J.B., Summer, E.J., Clare, M.A., Talling, P.J., Parsons, D.R., Cooper, C., 2017. A general model for the helical structure of geophysical flows in channel bends. Geophysical Research Letters 44 (23), 932–941.

Babonneau, N., Savoye, B., Cremer, M., Bez, M., 2004. Multiple terraces within the deep incised Zaire Valley (ZaiAngo Project): are they confined levees? Geological Society, London, Special Publications 222, pp. 91–114
Barrera, R., Reyes, G.A., Guzmán, G., Franco, J.V., 2001. Geología de la plancha 31 Campo de la Cruz, Escala 1:100000. Memoria explicativa, INGEOMINAS, Bogotá (In Spanish).
Bayet-Goll, A., Sharafi, M., Daraei, M., Nasiri, Y., 2023. The influence of hybrid sediment gravity flows on distribution and composition of trace-fossil assemblages: Ordovician succession of the north-eastern Alborz Range of Iran. Sedimentology 70 (3), 783–827.
Bayona, G., Cardona, A., Jaramillo, C., Mora, A., Montes, C., Valencia, V., Ayala, C., Montenegro, O., Ibañez, M., 2012. Early Paleogene magmatism in the northern Andes: insights on the effects of Oceanic Plateau–continent convergence. Earth and Planetary Science Letters 331–332, 97–111.
Bernal-Olaya, R., Mann, P., Escalona, A., 2015. Cenozoic tectonostratigraphic evolution of the Lower Magdalena Basin, Colombia: an example of an under– to overfilled forearc basin. In: Batolini, C., Mann, P. (Eds.), Petroleum Geology and Potential of the Colombian Caribbean Margin. 108, pp. 345–398.
Brandes, C., Winsemann, J., 2018. From incipient island arc to doubly-vergent orogen: a review of geodynamic models and sedimentary basin-fills of southern Central America. Island Arc 27 (5), e12255. https://doi.org/10.1111/iar.12255.
Brooks, H.K., Ito, M., Zuchuat, V., Peakall, J., Hodgson, D.M., 2022. Channel-lobe transition zone development in tectonically active settings: implications for hybrid bed development. The Depositional Record 8, 829–868.
Brooks, H.L., Hodgson, D.M., Brunt, R.L., Peakall, J., Hofstra, M., Flint, S.S., 2018. Deepwater channel-lobe transition zone dynamics: processes and depositional architecture, an example from the Karoo Basin. South Africa. GSA Bulletin 130, 1723–1746.
Callow, R.H.T., Kneller, B., Dykstra, M., McIlroy, D., 2014. Physical, biological, geochemical and sedimentological controls on the ichnology of submarine canyon and slope channel systems. Marine and Petroleum Geology 54, 144–166.
Cardona, A., Weber, M., Valencia, V., Bustamante, C., Montes, C., Cordani, U., Muñoz, C.M., 2012. Geochronology and geochemistry of the Parashi granitoid, NE Colombia: tectonic implication of short-lived Early Eocene plutonism along the SE Caribbean margin. Journal of South American Earth Sciences 50, 75–92.
Cartigny, M.J.B., Ventra, D., Postma, G., Van Den Berg, J.H., 2014. Morphodynamics and sedimentary structures of bedforms under supercritical-flow conditions: new insights from flume experiments. Sedimentology 61, 712–748.
Celis, S.A., Rodríguez-Tovar, F.J., Giraldo-Villegas, C.A., Pardo-Trujillo, A., 2021. Evolution of a fluvial-dominated delta during the Oligocene of the Colombian Caribbean: sedimentological and ichnological signatures in well-cores. Journal of South American Earth Sciences 111, 103440. https://doi.org/10.1016/j.jsames.2021.103440.
Celis, S.A., Rodríguez-Tovar, F.J., Pardo-Trujillo, A., García-García, F., Giraldo-Villegas, C.A., Gallego, F., Plata, A., Trejos-Tamayo, R., Vallejo-Hincapié, F., Cardona, J., 2023. Deciphering influencing processes in a tropical delta system (middle-late Eocene? to Early Miocene, Colombian Caribbean): signals from a well-core integrative sedimentological, ichnological, and micropaleontological analysis. Journal of South American Earth Sciences 127, 104368. https://doi.org/10.1016/j.jsames.2023.104368.
Chakraborty, C., Bose, P.K., 1992. Ripple/dune to upper stage plane bed transition: some observations from the ancient record. Geological Journal 27, 349–359.
Clark, J.D., Pickering, K.T., 1996. Submarine Channels: Processes and Architecture. Vallis Press, London.
Clavijo, J., Barrera, R., 2001. Geología de las planchas 44 Sincelejo y 52 Sahagún. Escala 1: 100.000. Memoria Explicativa. INGEOMINAS, Bogotá (In Spanish).
Cochrane, R., Spikings, R., Gerdes, A., Ulianov, A., Mora, A., Villagómez, D., Putlitz, B., Chiaradia, M., 2014. Permo-Triassic anatexis, continental rifting and the disassembly of western Pangaea. Lithos 190–191, 383–402.
Cornard, P.H., Pickering, K.T., 2019. Supercritical-flow deposits and their distribution in a submarine channel system, Middle Eocene, Ainsa Basin, Spanish Pyrenees. Journal of Sedimentary Research 89 (6), 576–597.
Covault, J.A., Kostic, S., Paull, C.K., Ryan, H.F., Fildani, A., 2014. Submarine channel initiation, filling and maintenance from sea-floor geomorphology and morphodynamic modelling of cyclic steps. Sedimentology 61, 1031–1054.
Dennielou, B., Droz, L., Jacq, C., Babonneau, N., Bonnel, C., Picot, M., Le Saout, M., Saout, J., Bez, M., Savoye, B., Olu, K., Rabouille, C., 2017. Morphology, structure, composition and build-up processes of the active Congo channel-mouth lobe complex with inputs from remotely operated underwater vehicle (ROV) multibeam and video surveys. Deep Sea Research Part II: Topical Studies in Oceanography 142, 25–49.
Domínguez-Giraldo, V., Arias-Díaz, A., Vallejo-Hincapié, F., Plata-Torres, A., Gallego, N.F., Pardo-Trujillo, A., 2023. Middle-late Eocene to Early Miocene micropaleontology of the ANH–TIERRALTA–2–X–P well: biostratigraphic implications for southwestern deposits of the Sinú-San Jacinto belt (Colombian Caribbean). Journal of South American Earth Sciences 128, 104420. https://doi.org/10.1016/j.jsames.2023.104547.
Duarte, L.M., 1997. L'Eocène et le Miocène du Bassin de la Vallèe Infèrieure de la Magdalena, Colombie: Sédimentologie, Litho- et Argilostratigraphie, Paléogéographie et Paleoclimatologie. University of Liège, Belgium (PhD thesis, 128 pp. In French).
Duque-Caro, H., 1979. Major structural elements and evolution of northwestern Colombia. In: Watkins, J.S., Montadert, L., Dickerson, P.W. (Eds.), Geological and Geophysical Investigations of Continental Margins. AAPG Memoir vol. 29, pp. 329–351.
Duque-Caro, H., 1984. Structural style, diapirism and accretionary episodes of the Sinú-San Jacinto terrane, southwestern Caribbean borderland. GSA Memoir 162, 303–316.
Duque-Caro, H., Guzmán Ospitia, G., Hernández, R., 1996. Geología de la plancha 38 Carmen de Bolívar, Escala 1:100.000. Instituto Colombiano de Geología y Minería INGEOMINAS, Bogotá 96 pp. (In Spanish).
Duque-Castaño, M., Trejos-Tamayo, R., Osorio-Tabares, L.C., Angulo-Pardo, E., Vallejo, F., Plata, A., Pardo-Trujillo, A., 2023. Lower to Middle Miocene multiproxy biostratigraphy of the P-18 core-stratigraphic well in Sinú-San Jacinto Basin, Caribbean region of Colombia. Journal of South American Earth Sciences 123, 104228. https://doi.org/10.1016/j.jsames.2023.104228.
Fedele, J.J., Hoyal, D.C., Barnaal, Z., Tulenko, J., Awalt, S., 2016. Bedforms created by gravity flows. In: Budd, D., Hajek, E., Purkis, S. (Eds.), Autogenic Dynamics and Self-organization in Sedimentary Systems. SEPM, Special Publications 106, pp. 95–121.
Fielding, C.R., 2006. Upper flow regime sheets, lenses and scour fills: extending the range of architectural elements for fluvial sediment bodies. Sedimentary Geology 190, 227–240.
Fildani, A., Normark, W.R., Kostic, S., Parker, G., 2006. Channel formation by flow stripping: large-scale scour features along the Monterey East Channel and their relation to sediment waves. Sedimentology 53, 1265–1287.
Fildani, A., Kostic, S., Covault, J.A., Maier, K.L., Caress, D.W., Paull, C.K., 2021. Exploring a new breadth of cyclic steps on distal submarine fans. Sedimentology 68, 1378–1399.
Flinch, J.F., 2003. Structural evolution of the Sinú-Lower Magdalena Area (Northern Colombia). In: Bartolini, C., Buffler, R.T., Blickwede, J. (Eds.), The Circum-Gulf of Mexico and the Caribbean: Hydrocarbon Habitats, Basin Formation, and Plate Tectonics. AAPG Memoir vol. 79, pp. 776–796.
Gábris, G., Nagy, B., 2005. Climate and tectonically controlled river style changes on the Sajó-Hernád alluvial fan (Hungary). In: Harvey, A.M., Mather, A.E., Stokes, M. (Eds.), Alluvial Fans: Geomorphology, Sedimentology, Dynamics. Geological Society, London, Special Publications, pp. 61–67.
Garzón Oyola, D.M., 2023. Reconstrucción paleoambiental entre el Eoceno tardío y el Mioceno Temprano en el Cinturón Plegado de San Jacinto (Caribe colombiano) a partir de foraminíferos bentónicos. University of Caldas, Colombia M.Sc thesis, 190 pp. In Spanish.
Ge, Z., Nemec, W., Vellinga, A.J., Gawthorpe, R.L., 2022. How is a turbidite actually deposited? Science Advances 8 (3), eabl9124. https://doi.org/10.1126/sciadv.abl9124.
Giraldo-Villegas, C.A., Rodríguez-Tovar, F.J., Celis, S.A., Pardo-Trujillo, A., Duque-Castaño, M.L., 2023. Paleoenvironmental conditions over the Caribbean Large Igneous Province during the Late Cretaceous in NW of South American Margin: a sedimentological and ichnological approach. Cretaceous Research 142, 105407. https://doi.org/10.1016/j.cretres.2022.105407.
Gladstone, C., McClelland, H.L., Woodcock, N.H., Pritchard, D., Hunt, J.E., 2018. The formation of convolute lamination in mud-rich turbidites. Sedimentology 65, 1800–1825.
Gómez, J., Montes, N.E., Nivia, Á., Diederix, H., 2015. Mapa Geológico de Colombia 2015. Escala 1:1 000 000. Ingeominas, Bogotá (In Spanish).
Gong, C., Chen, L., West, L., 2017. Asymmetrical, inversely graded, upstream-migrating cyclic steps in marine settings: Late Miocene-early Pliocene Fish Creek-Vallecito Basin, southern California. Sedimentary Geology 360, 35–46.
Grundvåg, S.-A., Helland-Hansen, W., Johannssen, E.P., Eggenhuisen, J., Pohl, F., Spychala, Y., 2023. Deep-water sand transfer by hyperpycnal flows, the Eocene of Spitsbergen, Arctic Norway. Sedimentology https://doi.org/10.1111/sed.13105.
Guzmán, G., 2007. Stratigraphy and Sedimentary Environment and Implications in the Plato Basin and the San Jacinto Belt Northwestern Colombia. University of Liège, Belgium (PhD thesis, 185 pp.).
Hage, S., Cartigny, M.J.B., Clare, M.A., Sumner, E.J., Vendettuoli, D., Hughes Clarke, J.E., Hubbard, S.M., Talling, P.J., Lintern, D.G., Stacey, C.D., Englert, R.G., Vardy, M.E., Hunt, J.E., Yokokawa, M., Parsons, D.R., Hizzett, J.L., Azpiroz-Zabala, M., Vellinga, A.J., 2018. How to recognize crescentic bedforms formed by supercritical turbidity currents in the geologic record: insights from active submarine channels. Geology 46 (6), 563–566.
Hand, B.M., 1974. Supercritical flow in density currents. Journal of Sedimentary Petrology 44, 637–648.
Hansen, L.A.S., Callow, R.H.T., Kane, I., Gamberi, F., Rovere, M., Cronin, B.T., Kneller, C., 2015. Genesis and character of thin-bedded turbidites associated with submarine channels. Marine and Petroleum Geology 67, 852–879.
Hansen, L.A.S., Healy, R.S., Gomis-Cartesio, L., Lee, D.R., Hodgson, D.M., Pontén, A., Wild, R. J., 2021. The origin and 3D architecture of a km-scale deep-water scour-fill: example from the Skoorsteenberg Fm, Karoo Basin, South Africa. Frontiers in Earth Science 9, 737932. https://doi.org/10.3389/feart.2021.737932.
Heard, T.G., Pickering, K.T., 2008. Trace fossils as diagnostic indicators of deep-marine environments, middle Eocene Ainsa-Jaca basin, Spanish Pyrenees. Sedimentology 55, 809–844.
Hodgson, D.M., Peakall, J., Maier, K.L., 2022. Submarine channel mouth settings: processes, geomorphology, and deposits. Frontiers in Earth Science 10, 790320. https://doi.org/10.3389/feart.2022.790320.
Hofstra, M., Hodgson, D.M., Peakall, J., Flint, S.S., 2015. Giant scour-fills in ancient channel-lobe transition zones: formative processes and depositional architecture. Sedimentary Geology 329, 98–114.
Hofstra, M., Peakall, J., Hodgson, D., Stevenson, C.J., 2018. Architecture and morphodynamics of subcritical sediment waves in an ancient channel-lobe transition zone. Sedimentology 65, 2339–2367.
Hubbard, S.M., Romans, B.W., Graham, S.A., 2008. Deep-water foreland basin deposits of the Cerro Toro Formation, Magallanes basin, Chile: architectural elements of a sinuous basin axial channel belt. Sedimentology 55 (5), 1333–1359.
Hubbard, S.M., de Ruig, M.J., Graham, S.A., 2009. Confined channel-levee complex development in an elongate depo-center: deep-water Tertiary strata of the Austrian Molasse basin. Marine and Petroleum Geology 26 (1), 85–112.
Hubbard, S.M., MacEachern, J.A., Bann, K.L., 2012. Slopes (chapter 20). In: Knaust, D., Bromley, R.G. (Eds.), Trace Fossils as Indicators of Sedimentary Environments, Developments in Sedimentology. vol. 64. Elsevier, Amsterdam, pp. 607–642.
Hughes Clarke, J.E., 2016. First wide-angle view of channelized turbidity currents links migrating cyclic steps to flow characteristics. Nature Communications 1–13.
Hughes Clarke, J.E., Shor, A.N., Piper, D.J.W., Mayer, L.A., 1990. Large-scale current-induced erosion and deposition in the path of the 1929 Grand Banks turbidity current. Sedimentology 37, 613–629.
Ito, M., Ishikawa, K., Nishida, N., 2014. Distinctive erosional and depositional structures formed at a canyon mouth: a lower Pleistocene deep-water succession in the Kazusa forearc basin on the Boso Peninsula, Japan. Sedimentology 61, 2042–2062.

Kane, I.A., Hodgson, D.M., 2011. Sedimentological criteria to differentiate submarine channel levee sub environments: exhumed examples from the Rosario Fm. (Upper Cretaceous) of Baja California, Mexico, and the Fort Brown Fm. (Permian), Karoo Basin, S. Africa. Marine and Petroleum Geology 28, 807–823.
Kane, I.A., Dykstra, M.L., Kneller, B.C., Tremblay, S., McCaffrey, W.D., 2009. Architecture of a coarse-grained channel-levee system: the Rosario Formation, Baja California, Mexico. Sedimentology 56, 2207–2234.
Kenyon, N.H., Amir, A., Cramp, A., 1995. Geometry of the younger sediment bodies of the Indus Fan. In: Pickering, K.T., Hiscott, R.N., Kenyon, N.H., Lucchi, R.R., Smith, R.D.A. (Eds.), Atlas of Deep-Water Environments: Architectural Style in Turbidite Systems. Chapman and Hall, London, pp. 89–93.
Kneller, B., Buckee, C., 2000. The structure and fluid mechanics of turbidity currents: a review of some recent studies and their geological implications. Sedimentology 47, 62–94.
Kneller, B.C., Branney, M.J., 1995. Sustained high density turbidity currents and the deposition of thick massive sands. Sedimentology 42, 607–616.
Kneller, B.C., McCaffrey, W.D., 2003. The interpretation of vertical sequences in turbidite beds: the influence of longitudinal flow structure. Journal of Sedimentary Research 73, 706–713.
Komar, P.D., 1985. The hydraulic interpretation of turbidites from their grain sizes and sedimentary structures. Sedimentology 32 (3), 395–407.
Lang, J., Winsemann, J., 2013. Lateral and vertical facies relationships of bedforms deposited by aggrading supercritical flows: from cyclic steps to humpback dunes. Sedimentary Geology 296, 36–54.
Lang, J., Brandes, C., Winsemann, J., 2017. Erosion and deposition by supercritical density flows during channel avulsion and backfilling: field examples from coarse-grained deepwater channel-levée complexes (Sandino Forearc Basin, southern Central America). Sedimentary Geology 349, 79–102.
Lang, J., Fedele, J.J., Hoyal, D.C., 2021. Three-dimensional submerged wall jets and their transition to density flows: morphodynamics and implications for the depositional record. Sedimentology 68 (4), 1297–1327.
León, S., Cardona, A., Parra, M., Robel, E.R., Jaramillo, J.S., Glodny, J., Valencia, V.A., Chew, D., Montes, C., Posada, G., Monsalve, G., Pardo-Trujillo, A., 2018. Transition from collisional to subduction-related regimes: an example from Neogene Panama-Nazca-South America interactions. Tectonics 37 (1), 119–139.
Lowe, D.R., 1976. Grain flow and grain flow deposits. Journal of Sedimentary Petrology 46, 188–199.
Lowe, D.R., 1982. Sediment gravity flows; II, depositional models with special reference to the deposits of high-density turbidity currents. Journal of Sedimentary Research 52 (1), 279–297.
Maestrelli, D., Maselli, V., Kneller, B., Chiarella, D., Scarselli, N., Vannuchi, P., Jovane, L., Iacopini, D., 2020. Characterisation of submarine depression trails driven by upslope migrating cyclic steps: insights from the Ceará Basin (Brazil). Marine and Petroleum Geology 115, 104291. https://doi.org/10.1016/j.marpetgeo.2020.104291.
Maier, K.L., Fildani, A., Paull, C.K., Grahan, S.A., McHargue, T.R., Caress, D.W., McGann, M., 2011. The elusive character of discontinuous deep-water channels: new insights from Lucia Chica channel system, offshore California. Geology 39 (4), 327–330.
Maier, K.L., Johnson, S.Y., Hart, P., 2018. Controls on submarine canyon head evolution, migration, and fill in Monterey Bay, offshore Central California. Marine Geology 404, 24–40.
Maier, K.L., Paull, C.K., Caress, D.W., Anderson, K., Nieminski, N.M., Lundsten, E., Erwin, B.E., Gwiazda, R., Fildani, A., 2020. Submarine-fan development revealed by integrated high-resolution datasets from La Jolla Fan, offshore California, USA. Journal of Sedimentary Research 90, 468–479.
Mann, P., 2021. Gulf of Mexico, Central America, and the Caribbean. In: Aldaberto, D., Elias, S.A. (Eds.), Encyclopedia of Geology, Second edition, pp. 47–67.
Mantilla-Pimiento, A., Jentzsch, G., Kley, J., Alfonso-Pava, C., 2009. Configuration of the Colombian Caribbean Margin: constraints from 2D seismic reflection data and potential fields interpretation. In: Lallemand, S., Funiciello, F. (Eds.), Subduction Zone Geodynamics. Frontier in Earth Sciences, pp. 247–272.
Martínez, C., Jaramillo, C., Martínez-Murcia, J., Crepet, W., Cárdenas, A., Escobar, J., Moreno, F., Pardo-Trujillo, A., Caballero-Rodríguez, D., 2021. Paleoclimatic and paleoecological reconstruction of a middle to late Eocene South American tropical dry forest. Global and Planetary Change 205, 103617. https://doi.org/10.1016/j.gloplacha.2021.103617.
Mayall, M., Jones, Ed, Casey, M., 2006. Turbidite channel reservoirs—key elements in facies prediction and effective development. Marine and Petroleum Geology 23 (8), 821–841.
McArthur, A., Kane, I., Bozetti, G., Hansen, L., Kneller, B.C., 2020. Supercritical flows overspilling from bypass-dominated submarine channels and the development of overbank bedforms. The Depositional Record 6, 21–40.
Mejía-Molina, A., Flores, J.A., Torres Torres, V., Sierro, F.J., 2010. Distribution of calcareous nannofossils in Upper Eocene-Upper Miocene deposits from Northern Colombia and the Caribbean Sea. Revista Española de Micropaleontología 42 (3), 279–300.
Montes, C., Guzman, G., Bayona, G., Cardona, A., Valencia, V., Jaramillo, C., 2010. Clockwise rotation of the Santa Marta massif and simultaneous Paleogene to Neogene deformation of the Plato-San Jorge and Cesar-Rancheria basins. Journal of South American Earth Sciences 29 (4), 832–848.
Montes, C., Rodriguez-Corcho, A.F., Bayona, G., Hoyos, N., Zapata, S., Cardona, A., 2019. Continental margin response to multiple arc–continent collisions: the northern Andes–Caribbean margin. Earth Science Reviews 198, 102903. https://doi.org/10.1016/j.earscirev.2019.102903.
Mora, J.A., Oncken, O., Le Breton, E., Ibánez-Mejia, M., Faccena, C., Veloza, G., Vélez, V., de Freitas, M., Mesa, A., 2017. Linking Late Cretaceous to Eocene tectonostratigraphy of the San Jacinto fold belt of NW Colombia with Caribbean plateau collision and flat subduction. Tectonics 36, 2599–2629.
Mora, J.A., Oncken, O., Le Breton, E., Mora, A., Veloza, G., Vélez, V., de Freitas, M., 2018. Controls on forearc basin formation and evolution: insights from Oligocene to Recent tectonostratigraphy of the Lower Magdalena Valley basin of Northwest Colombia. Marine and Petroleum Geology 97, 288–310.
Mora-Bohórquez, J.A., Oncken, O., Le Breton, E., Ibánez-Mejia, M., Veloza, G., Mora, A., Vélez, V., de Freitas, M., Gómez, J., Mateus-Zabala, D., 2020. Formation and evolution of the Lower Magdalena Valley Basin and San Jacinto Fold Belt of Northwestern Colombia: insights from upper Cretaceous to Recent Tectono–Stratigraphy. The Geology of Colombia, Volume 3 Paleogene – Neogene. Servicio Geológico Colombiano, Publicaciones Geológicas Especiales 37, pp. 21–66.
Mora-Páez, H., Kellogg, J.N., Freymueller, J., Mencin, D., Fernandes, R.M.S., Diederix, H., LaFemina, P., Cardona-Piedrahita, L., Lizarazo, S., Peláez-Gaviria, J.-R., Díaz-Mila, F., Bohórquez-Orozco, O., Giraldo-Londoño, L., Corchuelo-Cuervo, Y., 2019. Crustal deformation in the northern Andes – a new GPS velocity field. Journal of South American Earth Sciences 89, 76–91.
Mukti, M.M., Ito, M., 2010. Discovery of outcrop-scale fine-grained sediment waves in the lower Halang Formation, an upper Miocene submarine-fan succession in West Java. Sedimentary Geology 231, 55–62.
Mulder, T., Alexander, J., 2001. The physical character of subaqueous sedimentary density flows and their deposits. Sedimentology 49, 269–299.
Mulder, T., Syvitski, J.P.M., Migeon, S., Faugeres, J.C., Savoye, B., 2003. Marine hyperpycnal flows: initiation, behavior and related deposits: a review. Marine and Petroleum Geology 20, 861–882.
Mutti, E., 1992. Turbidite Sandstones. Universitá di Parma, Agip, San Donato, Milanese (275 pp.).
Mutti, E., Normark, W.R., Leggett, J.K., 1987. Comparing examples of modern and ancient turbidite systems: problems and concepts. In: Zuffa, G.G. (Ed.), Marine Clastic Sedimentology. Springer, The Netherlands, pp. 1–38.
Navarro, L., Arnott, R.W.B., 2020. Stratigraphic record in the transition from basin floor to continental slope sedimentation in the ancient passive-margin Windermere turbidite system. Sedimentology 67, 1710–1749.
Nemec, W., Steel, R.J., 1984. Alluvial and coastal conglomerates: their significant features and some comments on gravelly mass-flow dep osits. In: Koster, E.H., Steel, R.J. (Eds.), Sedimentology of Gravels and Conglomerates. Canadian Society of Petroleum Geologists Memoir vol. 10, pp. 1–31.
Nichols, G., 2009. Sedimentology and Stratigraphy. Blackwell Publishing, A John Wiley and Sons, Ltd., Publication (432 pp.).
Normark, W.R., Paull, C.K., Caress, D.W., Ussler III, W., Sliter, R., 2009. Fine-scale relief related to Late Holocene channel shifting within the floor of the upper Redondo Fan, offshore Southern California. Sedimentology 56, 1690–1704.
Ono, K., Plink-Bjorklund, P., 2018. Froude supercritical flow bedforms in deepwater slope channels? Field examples in conglomerates, sandstones and fine-grained deposits. Sedimentology 65, 639–669.
Ono, K., Plink-Bjorklund, P., Eggenhuisen, J.T., Cartigny, M.J.B., 2021. Froude supercritical flow processes and sedimentary structures: new insights from experiments with a wide range of grain sizes. Sedimentology 68 (4), 1328–1357.
Osorio-Granada, E., Pardo-Trujillo, A., Restrepo-Moreno, S.A., Gallego, F., Muñoz, J., Plata, A., Trejos-Tamayo, R., Vallejo, F., Barbosa-Espitia, A., Cardona-Sánchez, F.J., Foster, D.A., Kamenov, G., 2020. Provenance of Eocene-Oligocene sediments in the San Jacinto Fold Belt: paleogeographic and geodynamic implications for the northern Andes and the southern Caribbean. Geosphere 16 (1), 210–228.
Ospina-Muñoz, A., Marquez, I., Vallejo-Hincapié, F., Salazar-Ríos, A., Trejos-Tamayo, R., Celis, S.A., Plata, A., Pardo-Trujillo, A., 2023. Calcareous microfossil biostratigraphy of Upper Miocene to Pliocene deposits of the Sinú-San Jacinto Belt, Caribbean region of Colombia. Journal of South American Earth Sciences 129, 104468. https://doi.org/10.1016/j.jsames.2023.104468.
Palanques, A., Kenyon, N.H., Alonso, B., Limonov, A., 1995. Erosional and depositional patterns in the Valencia Channel mouth: an example of a modern channel-lobe transition zone. Marine Geophysical Researches 17, 503–517.
Parker, G., García, M., Fukushima, Y., Yu, W., 1987. Experiments on turbidity currents over an erodible bed. Journal of Hydraulic Research 25 (1), 123–147.
Paull, C., Caress, D., Lundsten, E., Gwiazda, R., Anderson, K., McGann, M., Conrad, J., Edwards, B., Sumner, E., 2013. Anatomy of the La Jolla submarine Canyon system; offshore southern California. Marine Geology 335, 16–34.
Peakall, J., Best, J., Baas, J.H., Hodgson, D.M., Clares, M.A., Talling, P.J., Dorrell, R.M., Lee, D.R., 2020. An integrated process-based model of flutes and tool marks in deep-water environments: implications for palaeohydraulics, the Bouma sequence and hybrid event beds. Sedimentology 67, 1601–1666.
Pemberton, E.A.L., Hubbard, S.M., Fildani, A., Romans, B., Straight, L., 2016. The stratigraphic expression of decreasing confinement along a deep-water sediment routing system: outcrop example from southern Chile. Geosphere 12 (1), 114–134.
Pickering, K.T., Hiscott, R.N., 2015. Deep Marine Systems: Processes, Deposits, Environments, Tectonics and Sedimentation. American Geophysical Union, Wiley, p. 696.
Pickering, K.T., Clark, J.D., Smith, R.D.A., Hiscott, R.N., Ricci Lucchi, F., Kenyon, N.H., 1995. Architectural element analysis of turbidite systems, and selected topical problems for sand-prone deep-water systems. In: Pickering, K.T., Hiscott, R.N., Kenyon, N.H., Lucchi, R., Smith, R.D.A. (Eds.), Atlas of Deep-water Environments; Architectural Style in Turbidite Systems. Chapman and Hall, London, pp. 1–10.
Pindell, J., Kennan, L., Maresch, W.V., Draper, G., 2005. Plate–kinematics and crustal dynamics of circum–Caribbean arc–continent interactions: tectonic controls on basin development in Proto–Caribbean margins. Geological Society of America Special Papers 394 (1), 7–52.
Pindell, J.L., Kennan, L., 2009. Tectonic evolution of the Gulf of Mexico, Caribbean and northern South America in the mantle reference frame: an update. In: James, K.H., Lorente, M.A., Pindell, J.L. (Eds.), The Origin and Evolution of the Caribbean Plate. Geological Society, London, Special Publicationsvol. 328, pp. 1–55.

Plata-Torres, A., Pardo-Trujillo, A., Vallejo-Hincapié, F., Trejos-Tamayo, R., Flores, J.A., 2023. Early Eocene (Ypresian) palynology of marine sediments from the colombian Caribbean. Journal of South American Earth Sciences 121, 104146. https://doi.org/10.1016/j.jsames.2022.104146.
Ponce, J.J., Carmona, N., 2011. Coarse-grained sediment waves in hyperpycnal clinoform systems, Miocene of the Austral foreland basin, Argentina. Geology 39 (8), 763–766.
Postma, G., Cartigny, M.J.B., 2014. Supercritical and subcritical turbidity currents and their deposits – a synthesis. Geology 42, 987–990.
Postma, G., Kleverlaan, K., 2018. Supercritical flows and their control on the architecture and facies of small-radius sand-rich fan lobes. Sedimentary Geology 364, 53–70.
Postma, G., Nemec, W., Kleinspehn, K.L., 1988. Large floating clasts in turbidites: a mechanism for their emplacement. Sedimentary Geology 58, 47–61.
Postma, G., Cartigny, M.J.B., Kleverlaan, K., 2009. Structureless, coarse-tail graded Bouma Ta formed by internal hydraulic jump of the turbidity current? Sedimentary Geology 219, 1–6.
Postma, G., Kleverlaan, K., Cartigny, M.J.B., 2014. Recognition of cyclic steps in sandy and gravelly turbidite sequences, and consequences for the Bouma facies model. Sedimentology 61, 2268–2290.
Postma, G., Hoyal, D.C., Abreu, V., Cartigny, M.J., Demko, T., Fedele, J.J., Kleverlaan, K., Pederson, K.H., 2016. Morphodynamics of supercritical turbidity currents in the channel-lobe transition zone. In: Lamarche, G., Moundjoy, J. (Eds.), Submarine Mass Movements and their Consequences. Advances in Natural and Technological Hazards Research. Springer, Dordrecht, pp. 469–478.
Postma, G., Lang, J., Hoyal, D.C., Fedele, J.J., Demko, T., Abreu, V., Pederson, K.H., 2021. Reconstruction of bedform dynamics controlled by supercritical flow in the channel-lobe transition zone of a deep-water delta (Sant Llorenç del Munt, north-east Spain, Eocene). Sedimentology 68 (4), 1–24.
Potter, P.E., Maynar, J., Depetris, P., 2005. Mud and Mudstones: Introduction and Overview. Springer, Berlin/Heidelberg, p. 305.
Restrepo-Moreno, S.A., Foster, D.A., Stockli, D.F., Parra-Sánchez, L.N., 2009. Long-term erosion and exhumation of the "Altiplano Antioqueño", Northern Andes (Colombia) from apatite (U-Th)/He thermochronology. Earth and Planetary Science Letters 278, 1–12.
Richards, M., Bowman, M., Reading, H., 1998. Submarine-fan systems i: characterization and stratigraphic prediction. Marine and Petroleum Geology 15 (7), 689–717.
Rincón-Martínez, D., Baumgartner, P.O., Sandoval, M.I., Restrepo-Acevedo, S.M., Baumgartner-Mora, C., 2023. Late Cretaceous and Paleocene radiolarians from the San Jacinto Fold Belt, Northeast Colombia: biostratigraphic and paleoenvironmental implications. Journal of South American Earth Sciences 126, 104325. https://doi.org/10.1016/j.jsames.2023.104325.
Rodríguez-Tovar, F.J., 2022. Ichnological analysis: a tool to characterize deep-marine processes and sediments. Earth-Science Reviews 228, 104014. https://doi.org/10.1016/j.earscirev.2022.104014.
Romito, S., Mann, P., 2020. Tectonic terranes underlying the present-day Caribbean plate: their tectonic origin, sedimentary thickness, subsidence histories and regional controls on hydrocarbon resources. In: Davison, I., Hull, J.N.F., Pindell, J. (Eds.), The Basins, Orogens and Evolution of the Southern Gulf of Mexico and Northern Caribbean. Geological Society, London, Special Publications 504 (1), p. 343.
Salazar-Ortiz, E., Numpaque, J., Bernal, L., Ocampo, E., Matajira, A., Villabona, J., Gómez, D., García, G., Méndez, S., Martínez, E., Sánchez, D., Sotelo, A.P., Aguirre, L., 2020a. Geología del área Sinú – San Jacinto, Planchas 23, 24, 30, 31 y parte de las planchas 37 y 38 a escala 1:50.000. Servicio Geológico Colombiano, Bogotá (In Spanish).
Salazar-Ortiz, E.A., Rincón-Martínez, D., Páez, L.-A., Restrepo, S.M., Barragán, S., 2020b. Middle Eocene mixed carbonate-siliciclastic systems in the southern Caribbean (NW Colombian margin). Journal of South American Earth Sciences 99, 102507. https://doi.org/10.1016/j.jsames.2020.102507.
Saunderson, H.C., Lockett, F.P.J., 1983. Flume experiments on bedforms and structures at the dune-plane bed transition. In: Collinson, J.D., Lewin, L. (Eds.), Modern and Ancient Fluvial Systems. Spec. International Association of Sedimentologists Special Publication vol. 6. Blackwell Science, Oxford, pp. 49–58.
Sequeiros, O.E., 2012. Estimating turbidity current conditions from channel morphology: a Froude number approach. Journal of Geophysical Research 117, C04003. https://doi.org/10.1029/2011JC007201.
Sequeiros, O.E., Spinewine, B., Beaubouef, R.T., Sun, T., García, M.H., Parker, G., 2010. Bedload transport and bed resistance associated with density and turbidity currents. Sedimentology 57, 1463–1490.
Silva, A., Paez, L., Rincon, M., Tamara, J., Gomez, P., Lopez, E., Restrepo, S., Mantilla, L., Valencia, V., 2017. Basement characteristics in the Lower Magdalena Valley and the Sinú and San Jacinto Fold belts: evidence of a Late Cretaceous magmatic arc at the south of the Colombian Caribbean: Ciencia. Tecnología y Futuro 6 (4), 5–36.
Slootman, A., Cartigny, M.J.B., 2020. Cyclic steps: review and aggradation-based classification. Earth-Science Reviews 201, 102949. https://doi.org/10.1016/j.earscirev.2019.102949.
Spikings, R., Cochrane, R., Villagomez, D., Van der Lelij, R., Vallejo, C., Winkler, W., Beate, B., 2015. The geological history of northwestern South America: from Pangaea to the early collision of the Caribbean Large Igneous Province (290–75Ma). Gondwana Research 27, 95–139.
Stevenson, C.J., Talling, P.J., Masson, D.G., Sumner, E.J., Frenz, M., Wynn, R.B., 2014. The spatial and temporal distribution of grain-size breaks in turbidites. Sedimentology 61, 1120–1156.
Stevenson, C.J., Jackson, C.A.L., Hodgson, D.M., Hubbard, S.M., Eggenhuisen, J.T., 2015. Deep-water sediment bypass. Journal of Sedimentary Research 85, 1058–1081.
Stow, D.A., Piper, D.J.W., 1984. Deep-water fine-grained sediments; history, methodology and terminology. Geological Society, London, Special Publications 15, 3–14.
Stow, D.A., Smillie, Z., 2020. Distinguishing between deep-water sediment facies: turbidites, contourites and hemipelagites. Geosciences 10, 1–43.
Stow, D.A.V., 1985. Fine-grained sediments in deep water: an overview of processes and facies models. Geo-Marine Letters 5, 17–23.
Stow, D.A.V., Tabrez, A., 1998. Hemipelagites: processes, facies and model. In: Stoker, M.S., Evans, D., Cramp, A. (Eds.), Geological Processes on Continental Margin: Sedimentation Mass-Wasting and Stability. Geological Society, London, Special Publicationsvol. 129, pp. 317–337.
Summer, E.J., Talling, P.J., Amy, L.A., Wynn, R.B., Stevenson, C.J., Frenz, M., 2012. Facies architecture of individual basin-plain turbidites: comparison with existing models and implications for flow processes. Sedimentology 59 (6), 1850–1887.
Symons, W.O., Sumner, E.J., Talling, P.J., Cartigny, M.J.B., Clare, M.A., 2016. Large-scale sediment waves and scours on the modern seafloor and their implications for the prevalence of supercritical flow. Marine Geology 371, 130–148.
Talling, P.J., Masson, D.G., Sumner, E.J., Malgesini, G., 2012. Subaqueous sediment density flows: depositional processes and deposit types. Sedimentology 59, 1937–2003.
Taylor, A.M., Goldring, R., 1993. Description and analysis of bioturbation and ichnofabric. Journal of the Geological Society of London 150, 141–148.
Tinterri, R., Civa, A., Laporta, M., Piazza, A., 2020. Turbidities and turbidity currents. In: Scarselli, N., Chiarella, D., Bally, A.W., Adam, J., Roberts, D.G. (Eds.), Regional Geology and Tectonics (Second Edition) Volume 1: Principles ofGeologic Analysis (Chapter 17, 39 pp.).
Tinterri, R., Mazza, T., Magalhaes, P.M., 2022. Contained-reflected megaturbidites of the Marnoso-arenacea Formation (Contessa Key Bed) and Helminthoid Flysches (Northern Apennines, Italy) and Hecho Group (South-Western Pyrenees). Frontiers in Earth Science 10, 817012. https://doi.org/10.3389/feart.2022.817012.
Uchman, A., 2009. The *Ophiomorpha rudis* ichnosubfacies of the *Nereites* ichnofacies: characteristics and constraints. Palaeogeography, Palaeoclimatology, Palaeoecology 276, 107–119.
Uchman, A., Wetzel, A., 2012. Deep-sea fans. In: Knaust, D., Bromley, R.G. (Eds.), Trace Fossils as Indicators of Sedimentary Environments. Developments i n Sedimentology vol. 64, pp. 643–671.
Vallejo-Hincapié, F., Flores, J.-A., Marie-Pierre, A., Pardo-Trujillo, A., 2023. Contribution to the Cenozoic chronostratigraphic framework of the Caribbean Sinú-San Jacinto Belt of Colombia based on calcareous nannofossils. Journal of South American Earth Sciences 127, 104419. https://doi.org/10.1016/j.jsames.2023.104419.
Van der Merwe, W., Hodgson, D.M., Brunt, R.L., Flint, S.S., 2014. Depositional architecture of sand-attached and sand-detached channel-lobe transition zones on an exhumed stepped slope mapped over a 2500 km2 area. Geosphere 10 (6), 1–18.
Vargas-González, V., Pardo-Trujillo, A., Gallego-Bañol, N.F., Restrepo-Moreno, S.A., Muñoz-Valencia, J.A., 2022. Procedencia de la Formación El Cerrito en el Cinturón Plegado de San Jacinto: implicaciones paleogeográficas para el Caribe colombiano. Boletín de Geología 44 (3), 39–63 (In Spanish).
Vellinga, A.J., Cartigny, M.J.B., Eggenhuisen, J.T., Hansen, E.W.M., 2018. Morphodynamics and depositional signature of low-aggradation cyclic steps: new insights from a depth-resolved numerical model. Sedimentology 65, 540–560.
Villagómez, D., Spikings, R., 2013. Thermochronology and tectonics of the Central and Western Cordilleras of Colombia: early Cretaceous–Tertiary evolution of the northern Andes. Lithos 160, 228–249.
Villagómez, D., Spikings, R., Magna, T., Kammer, A., Winkler, W., Beltrán, A., 2011. Geochronology, geochemistry and tectonic evolution of the Western and Central cordilleras of Colombia. Lithos 125, 875–896.
Wagreich, M., Strauss, P.E., 2005. Source area and tectonic control on alluvial-fan development in the Miocene Fohnsdorf intramontane basin, Austria. In: Harvey, A.M., Mather, A.E., Stokes, M. (Eds.), Alluvial Fans: Geomorphology, Sedimentology, Dynamics. Geological Society, London, Special Publications, pp. 207–216.
Walker, R.G., 1975. Generalized facies models for resedimented conglomerates of turbidite association. Geological Society of America Bulletin 86, 737–748.
West, L.M., Perillo, M.M., Olariu, C., Steel, R.J., 2019. Multi-event organization of deepwater sediments into bedforms: long-lived, large-scale antidunes preserved in deepwater slopes. Geology 47 (5), 391–394.
Wilkin, J., Cuthbertson, A., Dawson, S., Stow, D., Stephen, K., Nicholson, U., Penna, N., 2023. The response of high-density turbidity currents and their deposits to an abrupt channel termination at a slope break: implications for channel–lobe transition zones. Sedimentology 70, 1164–1194.
Winsemann, J., Lang, J., Fedele, J.J., Zavala, C., Hoyal, D.C., 2021. Re-examining models of shallow-water deltas: insights from tank experiments and field examples. Sedimentary Geology 421, 1–19.
Wynn, R.B., Kenyon, N.H., Masson, D.G., Stow, D.A.V., Weaver, P.P.E., 2002. Characterization and recognition of deepwater channel-lobe transition zones. AAPG Bulletin 86, 1441–1462.
Yang, T., Yingchang, C., Yanzhong, W., 2017. A new discovery of the Early Cretaceous supercritical hyperpycnal flow deposits on Lingshan Island, East China. Acta Geologica Sinica 91 (2), 749–750.
Zavala, C., 2020. Hyperpycnal (over density) flows and deposits. Journal of Paleogeography 9 (17) (21pp.).
Zavala, C., Pan, S.X., 2018. Hyperpycnal flows and hyperpycnites: origin and distinctive characteristics. Lithologic Reservoirs 3 (1), 1–27.
Zavala, C., Arcuri, M., Di Meglio, M., Gamero Diaz, H., Contreras, C., 2011. A genetic facies tract for the analysis of sustained hyperpycnal flow deposits. In: Slatt, R.M., Zavala, C. (Eds.), Sediment Transfer From Shelf to Deep Water Revisiting the Delivery System. AA PG Studies in Geology vol. 61, pp. 31–51.
Zavala, C., Arcuri, M., Blanco Valiente, L., 2012. The importance of plant remains as a diagnostic criteria for the recognition of ancient hyperpycnites. Revue de Paléobiologie 11, 457–469.